

HEAT STORAGE AND ENERGY CLOSURE IN TWO TROPICAL MONTANE FORESTS IN  
HAWAII

A THESIS SUBMITTED TO THE GRADUATE DIVISION OF THE UNIVERSITY OF HAWAII AT  
MĀNOA IN PARTIAL FULFILLMENT OF THE REQUIREMENTS FOR THE DEGREE OF

MASTER OF ARTS

IN

GEOGRAPHY

AUGUST 2012

By

Ryan G. Mudd

Thesis Committee:

Thomas Giambelluca, Chairperson

Ross Sutherland

Qi Chen

## ACKNOWLEDGEMENTS

Field data collection, screening and processing of data, and writing of this thesis was made possible by a motivated group of researchers for which I have been exceptionally grateful to work with. My advisor, Thomas Giambelluca was instrumental in securing funding for setup, maintenance and calibration of field instruments. He continued to source external resources to support me as a graduate research assistant, and I am grateful for the opportunity to work in a supportive and flexible learning environment. I would also like to thank Michael Nullet for invaluable assistance and advice concerning operation of meteorological sensors, field maintenance, and programming of dataloggers. Processing of 10 Hz eddy covariance data was carried out by Maoyi Huang, a critical and time consuming contribution to this work. Greg Asner provided the infrared gas analyzers used at the field research sites discussed herein, a vital contribution to the climate monitoring stations in Hawai'i Volcanoes National Park. John Delay, Mami Takahashi, and Roberta Martin contributed by conducting field biomass surveys, and their expertise in identifying and measuring plants contributed to the quality of the surveys. Committee members Ross Sutherland and Qi Chen contributed with their thorough comments and suggestions regarding improvement of this thesis. This research in Hawai'i Volcanoes National Park (HAVO) was facilitated by David Foote of the USGS Pacific Island Ecosystems Research Center and former and current Natural Resource Managers Tim Tunison and Rhonda Loh, Hawai'i, HAVO. Their hospitality and unrelenting support in hosting our research has been critical to the long-term maintenance of meteorological sensors and flux tower facilities in Hawai'i. Funding of this research was made possible by grants from the National Science Foundation Grant No. EAR-0309731, USGS Biological Resources Division Global Change Research Program, USGS Pacific Island Ecosystems Research Center, NSF Hawai'i EPSCoR Grant No. EPS-0903833, Pacific Islands Climate Change Cooperative Award No. FSR1-PICCC-FY2010, and USGS Water Resources Research Center project No.2008JI224B.

## ABSTRACT

Eddy covariance data collected above land surfaces provide direct measurements of evapotranspiration (ET), the sum of all evaporative processes over a particular land cover including transpiration, soil evaporation, and wet canopy evaporation, and a limited number of assessments of these data in tropical forests have been carried out. Evaluation of eddy covariance data is regularly conducted by assessing the energy balance, including radiation exchange measured above the vegetation and heat storage in the vegetation, soil, and the column of air below the eddy covariance sensors. In a native Hawaiian tropical montane forest (Nahuku) and a nearby forest (‘Ōla‘a) that has been partially invaded by strawberry guava (*Psidium cattleianum*), vertical and radial distribution of all biomass components were evaluated from detailed stand surveys, biomass samples, allometric relationships, wood density, fresh to dry weight ratios of plant materials, and temperature measurements of stem biomass. Eddy covariance data were analyzed at the two sites in Hawai‘i Volcanoes National Park, Hawai‘i, for a 34 month period to evaluate the importance of biomass and air heat storage to the energy balance and determine site specific energy closure characteristics. Total fresh biomass was estimated to be  $69.8 \pm 11.7 \text{ kg m}^{-2}$  and  $75.9 \pm 16.6 \text{ kg m}^{-2}$  at Nahuku and ‘Ōla‘a, respectively, and the contribution of separate biomass components to energy closure were evaluated in detail. Despite statistically similar fresh biomass between stands, energy storage was found to be significantly greater at the forest site with *P. cattleianum* tree invasion (‘Ōla‘a) than at the native *Metrosideros polymorpha* forest stand (Nahuku). The difference was attributed to a higher proportion of smaller stems at ‘Ōla‘a, absorbing and releasing more heat for a given mass. Inclusion of biomass and air heat storage in the energy balance improved the relative energy closure ( $\Omega$ ), the slope of the linear regression (forced through the origin) of the sum of latent and sensible heat fluxes measured above the canopies for each 30-minute period from 0.767 to 0.805 at Nahuku and from 0.918 to 0.997 at ‘Ōla‘a. The mean absolute energy imbalance ( $E_{\text{ABS}}$ ), the mean of the differences between the available energy and the sum of latent and sensible heat fluxes for each 30 minute interval for a binned group of values, was also reduced for most parts of the diurnal cycle. These results indicate that it is necessary to include heat storage in energy balance investigations to reduce error in energy balance adjustments of ET. However, it was found that the relative energy closure is not constant over all environmental conditions and has complex relationships with friction velocity, atmospheric

stability, and time of day. Therefore, energy closure adjustments to ET estimates should consider environmentally controlled variation in the relative and absolute energy closure in order to reduce error in estimates of land-atmosphere gas exchange. Furthermore, including all significant heat storage terms does not close the energy balance at the native forest site, which is likely due to additional site specific factors influencing the characteristics of turbulent flows over the surface.

## TABLE OF CONTENTS

ACKNOWLEDGMENTS.....	ii
ABSTRACT.....	iii
LIST OF TABLES.....	vii
LIST OF FIGURES.....	viii
LIST OF ABBREVIATIONS AND SYMBOLS.....	ix
<b>1. INTRODUCTION</b> .....	<b>1</b>
1.1 Problem and Objectives .....	1
1.2 Energy Closure at Eddy Covariance Sites .....	2
1.3 Heat Storage and Energy Closure.....	4
1.4 Estimation of Biomass Heat Storage .....	8
1.5 Gap-filling Latent and Sensible Heat Fluxes .....	10
1.6 Related Prior Research .....	11
<b>2. METHODS</b> .....	<b>12</b>
2.1 Overview.....	12
2.2 Site Descriptions.....	12
2.3 Meteorological Measurements.....	14
2.4 Survey Plots .....	15
2.5 Determination of Total Biomass - Allometric Models.....	16
2.6 Vertical and Radial Distribution of Stem Biomass.....	18
2.6.1 <i>Metrosideros polymorpha</i> and Other Native Trees .....	18
2.6.2 <i>Psidium cattleianum</i> .....	23
2.7 Modeling Stem Core Temperature.....	24
2.8 Vertical Distribution of Leaves and Epiphytes.....	26
2.9 Specific Heat of Biomass Components.....	26
2.10 Energy Storage in Biomass, Air, and Soil .....	27
2.11 Effects of Environmental Parameters on Energy Closure .....	29

<b>3. RESULTS</b> .....	31
3.1 Fresh Biomass Estimates .....	31
3.2 Temperature Measurements and Modeling .....	31
3.3 Heat Storage flux in the Biomass, Air, and Soil .....	32
3.4 Energy Closure and Heat Storage .....	33
3.5 Effects of Environmental Variability on Energy Closure .....	33
<b>4. DISCUSSION</b> .....	36
4.1 Evaluation of Fresh Biomass and Energy Storage Estimates .....	36
4.2 Energy closure in Relation to Environmental Variability .....	37
4.3 Gap-filling of Sensible and Latent Heat Fluxes .....	39
4.4 Evapotranspiration Adjustments Based on Energy Closure .....	41
<b>5. CONCLUSIONS</b> .....	41
<b>REFERENCES</b> .....	43
<b>TABLES</b> .....	50
<b>FIGURES</b> .....	56

## LIST OF TABLES

<b>Table</b>	<b>Description</b>	<b>Page</b>
2.1	Vegetation characteristics of canopy and subcanopy species in survey plots.....	50
2.2	Wood density (WD) and wet to dry ratio's ( $R_{WD}$ ) for stems and leaves.....	50
2.3	Regressions developed from harvested <i>Psidium cattleianum</i> trees.....	51
3.1	Fresh biomass ( $\text{kg m}^{-2}$ ) by component at Nahuku and 'Ōla'a .....	51
3.2	Radial and vertical distribution of fresh biomass.....	52
3.3	Parameters used to estimate energy storage in the annular portions of biomass.....	53
3.4	Parameters used to model temperature and energy storage in the interior volume of stems .....	54
4.1	Summary of reported heat storage fluxes and energy closure improvements ...	55

## LIST OF FIGURES

Figure	Description	Page
2.1	Stratified figure of mature <i>Metrosideros polymorpha</i> tree and the biomass height profile. ....	56
2.2	Cross-section of stem and variables used in radial separation of biomass .....	56
2.3	Evaluation of <i>Metrosideros polymorpha</i> allometry .....	57
2.4	$D_{BH}$ and dry biomass for all harvested <i>P. cattleianum</i> trees .....	57
3.1	Three-day sample period of stem temperature time series .....	58
3.2	Mean diurnal cycle of heat storage in the biomass, air, soil, and all components combined at both sites.....	58
3.3	Mean diurnal cycles of heat storage in biomass elements at both sites .....	59
3.4	Mean diurnal cycles of the vertical distribution of heat storage in the biomass and soil layer above the heat flux plates at both sites .....	59
3.5	Mean diurnal cycle of mass specific heat storage at different levels in the canopy and soil layer above the heat flux plates at both sites .....	59
3.6	Mean daytime and night-time course of the ratio of $Q_B$ , $Q_A$ , and $Q_{SUM}$ to $R_{NET} - G$ at both sites .....	60
3.7	Mean diurnal cycles of absolute energy imbalance before and after heat storage corrections at both sites.....	60
3.8	Relative energy closure at both sites for available radiation set to $R_{NET} - G$ and $R_{NET} - Q_{SUM}$ .....	61
3.9	Mean diurnal cycles of $u^*$ and $\xi$ at both sites .....	62
3.10	$\Omega$ and $E_{I_{ABS}}$ as a function of $u^*$ at both sites for available radiation set to $R_{NET} - G$ and $R_{NET} - Q_{SUM}$ for daytime and night-time periods .....	63
3.11	$\Omega$ and $E_{I_{ABS}}$ as a function of $\xi$ at both sites for available radiation set to $R_{NET} - G$ and $R_{NET} - Q_{SUM}$ .....	64
3.12	$\Omega$ according to time of day at both sites for available radiation set to $R_{NET} - G$ and $R_{NET} - Q_{SUM}$ .....	65

## LIST OF ABBREVIATIONS AND SYMBOLS

BA	basal area of each species, calculated using $D_{BH}$ measurements in survey plots ( $\text{cm}^2 \text{m}^{-2}$ )
$B_F$	stand level fresh biomass ( $\text{kg m}^{-2}$ )
$B_S$	stand fresh biomass of each biomass component or stem compartment ( $\text{kg m}^{-2}$ )
$B_{L\_MP}$	total leaf dry biomass for <i>M. polymorpha</i> ( $\text{kg tree}^{-1}$ )
$B_{T\_MP}$	total stem and leaf aboveground dry biomass for <i>M. polymorpha</i> ( $\text{kg tree}^{-1}$ )
$B_{L\_PC}$	leaf dry biomass for <i>P. cattleianum</i> ( $\text{g tree}^{-1}$ )
$B_{TW}$	twig dry biomass ( $\text{g tree}^{-1}$ )
$C_{CEL}$	specific heat of cellulose ( $\text{J kg}^{-1} \text{°C}^{-1}$ )
$q_{VEG}$	moisture content of vegetation (mass of water / mass of dry vegetation)
$C_W$	specific heat of water vapor ( $4186 \text{ J kg}^{-1} \text{°C}^{-1}$ )
$C_B$	specific heat of each biomass component ( $\text{J kg}^{-1} \text{°C}^{-1}$ )
$C_P$	specific heat of dry air ( $1004 \text{ J kg}^{-1} \text{°C}^{-1}$ )
$C_S$	specific heat for mineral soil ( $\text{J kg}^{-1} \text{°C}^{-1}$ )
CWD	coarse woody debris (fallen stems greater than 5 cm diameter)
$D_{BH}$	diameter at breast height (1.3 m)
$D_{BH\_FIG}$	measured $D_{BH}$ of the enlarged Figure 1a (cm)
$D_M$	measured midpoint diameter of each section in each stratum measured from the enlarged Figure 1a (cm)
dq	change in water vapor over the interval dt ( $\text{kg m}^{-3}$ )
dt	change in time between data averaging intervals (1800 s)
$dT_B$	change in temperature from the previous dt for each biomass component ( $\text{°C}$ )
$dT_{MC}$	change in modeled core temperature from the previous dt ( $\text{°C}$ )
$dT_{SOIL}$	two sensor average temperature change over the time interval dt ( $\text{°C}$ )
EBR	energy balance ratio $(LE + H) / (R_{NET} - Q_{SUM})$ over a given time period.
ET	sum of evaporation from wet surfaces and transpiration (mm)
$E_{ABS}$	mean absolute energy imbalance ( $\text{W m}^{-2}$ )
g	the acceleration of gravity ( $9.81 \text{ m s}^{-2}$ )
G	soil heat flux measured at 8 cm depth ( $\text{W m}^{-2}$ )
H	sensible heat flux to the atmosphere ( $\text{W m}^{-2}$ )
$H_T$	height of the temperature measurements (m)
$H_{t_{CANOPY}}$	mean canopy height (m)
$H_{t_{FIG}}$	total height of the enlarged Figure 2.1a (cm)
$H_{t_i}$	height of the bottom of each stratum for each tree (m)
$H_{t_j}$	height of the top of each stratum for each tree (m)
$H_{t_{OBS}}$	observation height where eddy covariance instruments are installed (m).
$H_{t_{RANGE}}$	height range where biomass was separately quantified (m)
$H_{t_{TREE}}$	estimated total tree height of each tree in the survey plot (m)
$H_V$	virtual sensible heat flux ( $\text{W m}^{-2}$ )
k	von Karman constant
L	Obukhov length scale (m)
lag	time lag of the rate of change of temperature with depth into the stem ( $\text{min cm}^{-1}$ )
litter	dead foliage and stems less than 5 cm
LE	latent energy flux ( $\text{W m}^{-2}$ )
$L_M$	length of the measured stem in the enlarged Figure 2.1a (cm)
$L_{STEM}$	length of each stem section for trees in the survey plot (cm)

p	period of oscillation (84,000 seconds for a diurnal cycle)
q	water vapor concentration ( $\text{kg m}^{-3}$ )
$Q_A$	combined $Q_H$ and $Q_{LE}$ in the air column below the eddy covariance sensors ( $\text{W m}^{-2}$ )
$Q_B$	change in energy storage in biomass ( $\text{W m}^{-2}$ )
$Q_H$	change in sensible heat storage in the air below the eddy covariance sensors ( $\text{W m}^{-2}$ )
$Q_{LE}$	change in latent energy storage in the air below the eddy covariance sensors ( $\text{W m}^{-2}$ )
$Q_S$	change in energy storage in the top 8 cm of soil above the heat flux plates ( $\text{W m}^{-2}$ ).
$Q_{SUM}$	change in energy storage in all above ground energy storage sinks ( $\text{W m}^{-2}$ )
$q_{VEG}$	moisture content of vegetation ( $\text{kg kg}^{-1}$ )
$r^2$	coefficient of determination of a regression
$R_1$	radius of each stem section for trees in the survey plot (cm)
$R_2$	core radius of each stem section for trees in the survey plot (cm)
RMSE	root mean square error of the regression between available energy and turbulent fluxes ( $\text{W m}^{-2}$ )
$R_{NET}$	net radiant flux density measured above the canopy ( $\text{W m}^{-2}$ )
$R_{T1}$	radius of the center of mass of $V_{SKIN}$ (cm)
$R_{T2}$	radius of the center of mass of $V_{CORE}$ (cm)
$S_B$	Standard error of the regression slope
$SHF_{1-4}$	outputs from 4 soil heat flux plates at 8 cm depth ( $\text{W m}^{-2}$ )
$T_A$	temperature anomaly - represents $dT_{MC}$ at depth $ZT_{MC}$ ( $^{\circ}\text{C}$ )
$T_{MC}$	modeled stem core temperature ( $^{\circ}\text{C}$ )
$TR_1$	mean diurnal temperature range measured at $ZT_S$ ( $^{\circ}\text{C}$ )
$TR_2$	mean diurnal temperature range of the deeper sensor measured at $ZT_C$ ( $^{\circ}\text{C}$ )
$TR_{MC}$	mean diurnal temperature range at $ZT_{MC}$ ( $^{\circ}\text{C}$ )
$T_S$	temperature measurement of the skin ( $^{\circ}\text{C}$ )
$\bar{T}_S$	mean $T_S$ for the entire period of analysis ( $^{\circ}\text{C}$ )
$T_{SKIN}$	measured temperature of $V_{SKIN}$ , the average of four skin temperature sensors at each measurement height ( $^{\circ}\text{C}$ )
$u^*$	friction velocity ( $\text{m s}^{-1}$ )
$V_{CORE}$	core volume of a section of stem ( $\text{cm}^3$ )
$V_{SKIN}$	skin volume of a section of stem ( $\text{cm}^3$ )
$V_{TOTAL}$	total volume of a section of stem ( $\text{cm}^3$ )
WD	wood density ( $\text{g cm}^{-3}$ )
$\bar{x}$	mean value of $R_{NET} - Q_{SUM}$ or $R_{NET} - G$ for each bin ( $\text{W m}^{-2}$ )
$x_i$	measured value of $R_{NET} - Q_{SUM}$ or $R_{NET} - G$ for each observation ( $\text{W m}^{-2}$ )
$y_i$	measured value of $LE + H$ for each observation $i$ ( $\text{W m}^{-2}$ )
$\hat{y}_i$	predicted value of $LE + H$ for each observation $i$ ( $\text{W m}^{-2}$ )
$z$	eddy covariance measurement height (m)
$z_0$	zero plane displacement height (m)
$z_A$	depth of the air layer under the eddy covariance instruments (m)
$z_{SOIL}$	depth of the storage layer above the heat flux plates (0.08 m)
$zT_C$	depth of core temperature measurement in stem (cm)
$zT_{MC}$	depth of modeled core temperature measurement (cm)
$zT_S$	depth at which outer temperature sensors are installed (cm)

### Greek letters

$\alpha$	thermal diffusivity (unitless)
$\xi$	stability parameter (unitless)
$\Omega$	relative energy closure; slope of the linear regression of available energy and the sum of LE and H for each 30 minute period
$\lambda$	latent heat of vaporization ( $\text{J kg}^{-1}$ )
$\theta_V$	virtual potential temperature at the surface (K)
$\rho_A$	air density ( $\text{kg m}^{-3}$ )
$\rho_{BD}$	soil bulk density ( $\text{kg m}^{-3}$ )
$\rho_{DRY}$	density of dry air ( $\text{kg m}^{-3}$ )
$\rho_W$	density of water (approximated as $1000 \text{ kg m}^{-3}$ )
$W_V$	volumetric soil moisture content ( $\text{m}^3 \text{ m}^{-3}$ )

## CHAPTER 1. INTRODUCTION

### 1.1 Energy Closure at Eddy Covariance Sites

Closing the energy balance over vegetated surfaces is a fundamental goal in studies that seek to measure ecosystem energy, water, and carbon exchange using the eddy covariance method. While eddy covariance measurements are commonly used for assessment of net ecosystem carbon exchange, global and regional water budgets gain valuable insight from direct measurements of vertical latent and sensible heat flux densities over vegetated surfaces because evapotranspiration (ET) estimates can be integrated over representative land cover types (Scott, 2010; Barr et al., 2011). Additionally, high temporal resolution measurements allow environmental controls on ecosystem processes to be investigated (Wilson and Baldocchi, 2000; Giambelluca et al., 2009; Kume et al., 2011). Land surface models of water and carbon exchange between the surface and the atmosphere depend on reliable landscape-scale validation to test simulations of regional and global scale climate models (Nagler et al., 2005; Reichstein et al., 2007; Jung et al., 2011), and regional networks of flux stations have been assembled for this purpose (ie. Ameriflux, Euroflux, Asiaflux, etc.), with an estimated 500 stations operated globally (Sulkava et al., 2011). Because sum of measured sensible and latent heat fluxes is usually less than the available energy (see discussion below), eddy covariance data is subject to scrutiny regarding the magnitude and sources of this discrepancy in the energy balance. Evaluation of eddy covariance data is routinely conducted by assessing the energy balance, including radiation exchange and storage of heat in vegetation and soil to assess the consistency of direct measurements of ET. However, the importance of evaluating heat storage as part of the energy balance closure process is not clearly known and the methods of doing so are not clearly defined.

The overall objective of this study is to determine, for two study sites, the effects of including biomass and air layer heat storage on the energy closure. This study also proposes and implements methods for determination of heat storage terms in the surface energy balance, and evaluates of the comparative contribution of various components of the biomass. The hypothesis is that inclusion of heat storage terms at 30 minute intervals will temporally align radiation measurements with direct measurements of fluxes through the diurnal course, reducing the magnitude of this discrepancy, thereby improving energy closure.

## 1.2. Energy Closure at Eddy Covariance Sites

The energy balance for an area of the earth's surface can be described as:

$$R_{\text{NET}} = LE + H + G + Q_S + Q_B + Q_A \quad [1]$$

where  $R_{\text{NET}}$  is the net radiant flux density measured above the canopy,  $LE$  is the latent energy flux,  $H$  is the sensible heat flux,  $G$  is the soil heat flux,  $Q_S$  is the heat storage flux in the layer of soil above the heat flux plates,  $Q_B$  is heat storage flux of above-ground fresh biomass, and  $Q_A$  is the combined sensible and latent storage flux ( $Q_H$  and  $Q_{LE}$ , respectively) in the air space beneath the eddy covariance sensors. The units for all terms are in  $\text{W m}^{-2}$ . Energy used for photosynthesis is assumed to be very small, and has been found to be less than 1 % relative to net radiation in tropical forests (Malhi et al., 2002) and other C3 plant canopies (Zhu et al., 2012), and will be omitted in this study.

Eddy covariance measurements of  $LE$  and  $H$  can be evaluated using the energy balance. Equation 1 is rearranged to set the available energy equal to the turbulent fluxes measured above the canopy:

$$R_{\text{NET}} - G - Q_S - Q_B - Q_A = LE + H \quad [2]$$

The relative energy closure ( $\Omega$ ) is evaluated as the slope of the simple linear regression of the right side vs. the left side of Equation 2 with turbulent fluxes at 30 minute intervals measured above the forest canopy ( $LE + H$ ) on the y-axis. The regression is often forced through the origin to give the relationship in the form of one coefficient, analogous to a ratio of the y variable to the x variable. Values of  $\Omega$  equal to one represent 1:1 energy closure (with some degree of variance in 30-minute values), while values of  $\Omega$  less than one, on average, represent an energy closure deficit. Values of  $\Omega$  greater than 1, while uncommon (Wilson et al., 2002), represent an energy surplus, meaning the measured turbulent fluxes are on average higher than net radiation and heat storage.

Measurements over vegetated surfaces typically display negative bias in energy balance using the eddy covariance method, i.e. the sum of measurements  $LE$  and  $H$  is usually less than the measured available energy on the order of 10–30 % (Wilson et al., 2002; Barr et al., 2006;

Hendricks Franssen et al., 2010). Assessments of measurements from across FLUXNET (Baldocchi et al., 2001) sites have highlighted the need for continued research concerning systematic and random error (Billesbach, 2011) and effects of apparent intrinsic lack of energy closure on ET and CO<sub>2</sub> fluxes. Errors associated with eddy covariance data collection are numerous (Massman and Lee, 2002). Many sources of error can be minimized during installation and operation of meteorological towers and sensors (Lee et al., 2004). Poorly calibrated meteorological sensors are a major concern regarding bias in the data, although this can be avoided by use of high quality sensors and timely maintenance and calibration. Divergence between radiation measurements from a meteorological tower and the radiation exchange of the spatially variable upwind area contributing to flux measurements can be minimized by carefully choosing a representative site for the meteorological tower location, and removing data when the wind direction is not from the target area. Removal of unreliable data when eddy covariance sensors are wet or for other reasons when the data may be unreliable may cause error in temporally integrated fluxes and gap filling strategies must be considered carefully. However errors caused by vegetation heterogeneity, changing upwind sources of turbulent fluxes, and instrumentation bias (sensor quality, calibration accuracy, and positioning) do not explain the consistent negative bias of energy closure at most sites (Foken, 2008).

Reasons for systematic errors in eddy covariance systems have been investigated in detail, and the majority of studies agree that turbulent flux measurements cannot capture surface atmosphere gas exchange in its entirety, and that complex terrain introduces atmospheric motions that violate assumptions regarding turbulent flux measurements. While multiple site analysis of eddy covariance data allows generalizations regarding energy imbalance to be made (Baldocchi et al., 2001; Barr et al., 2006; Moderow et al., 2009; Hendricks Franssen et al., 2010), each site is unique and demands careful vegetation surveys of the area under investigation.

Unaccounted advection of energy, water vapor, and carbon dioxide has been shown to be a factor contributing to bias in turbulent flux measurements (Moderow et al., 2007; Oncley et al., 2007; Leuning et al., 2008, Vickers et al., 2012). However, Thomas (2011) discussed that results of direct advection measurements, which are expensive and often impractical to implement at field research stations, might be ambiguous without dense spatial observation. Generally, advection is not directly measured in eddy covariance field studies and is minimized by selection of research sites over homogenous terrain. Nevertheless, the terrain over which

measurements are desired is not always flat, and advection may result from shallow downslope air flow induced by nocturnal cooling, possibly resulting in flux loss at the eddy covariance sensor level at the forested sites in Hawai'i referenced in this paper (particularly at Nahuku) due to somewhat sloping terrain (5%).

### 1.3 Heat Storage and Energy Closure

It has recently been argued that surface heat storage has a relatively insignificant effect on energy closure. According to a review on the energy closure problem by Foken (2008), the inherent loss is most likely due to larger turbulent structures because it was found that extending the averaging area (Kanda et al., 2004; Von Randow et al., 2008) or averaging time (Finnigan, 2003) of turbulent fluxes improves energy closure. Additionally, the averaging method may not be appropriate to represent the ensemble average vertical transport. Sakai et al. (2001) resolved energy imbalances at two dissimilar sites by normalizing cospectral similarity functions to describe momentum and scalar fluxes in the roughness sub-layer, and found relatively long period eddies (4–30 minutes) contribute significantly, indicating that large scale circulations cannot be ruled out at some sites. Hendricks Franssen et al. (2010) evaluated energy closure based on binned atmospheric stability ( $\xi$ , dimensionless), friction velocity ( $u^*$ ,  $\text{m s}^{-1}$ ), thermally induced turbulence, and time of day. They concluded that during conditions of near neutral  $\xi$ ,  $\Omega$  does not correspond to the relative energy closure deficit, which is much larger for these circumstances. The study revealed that filtering data for low  $u^*$  values as a means to remove periods where closure is poor is not necessarily effective, as other environmental factors such as the overall stability, the thermally induced turbulence, and time of day all have complex relationships with  $\Omega$ . They argued heat storage sinks play a relatively small role in regards to closing the energy balance. Considering previous independent studies that reveal improvement of energy closure when all storage terms are considered (Lamaud et al., 2001; Meyers and Hollinger, 2004; Haverd, 2007; Michiles and Gielow, 2008; Moderow et al., 2009; Lindroth et al., 2010; Wang and Zhang, 2011), it appears to be pre-mature to discount the influence of missing or haphazardly quantified heat storage sinks as a possible cause of poor energy closure at a particular site. Furthermore, Lindroth et al. (2010) reported that the absolute energy imbalance under stable atmospheric conditions (as indicated by the Richardson number) is reduced when heat storage terms are included. Hendricks Franssen et al. (2010) neglected heat storage terms

in evaluation of  $\Omega$  as a function of  $\xi$ . Because relatively few studies have considered the role of biomass heat storage in energy closure, more research is necessary concerning evaluation of the systematic energy imbalance found with eddy covariance flux estimates.

It is likely that the distribution of possible explanations for lack of energy closure is attributable to one or more site specific factors (Moderow et al., 2009), which makes it difficult to generalize the source of the problem, and emphasizes the importance of detailed site specific analysis in interpreting results clearly. A critical primary step in evaluating turbulent flux measurements at any site is a thorough evaluation of the energy balance and consideration of the potential contribution of different sources of error. If the error is assumed to be due to systematic underestimation of LE and H by eddy covariance measurement systems, it will be necessary to adjust turbulent flux measurements accordingly.

Forest canopies, especially in tropical environments have the potential to store large amounts of energy as heat (Moore and Fisch, 1986), affecting the energy balance measured above the canopy. If there is significant vegetation cover, it is important to carefully consider heat storage above-ground biomass. For tall meteorological towers, the latent and sensible heat stored in the airspace below the height of the eddy covariance sensors must be considered as well. While soil heat flux is less important with significant vegetation cover and more important in open canopies or over bare soil, evaluation of all heat storage terms is important to adjust the available energy and reduce error in the reported range of uncertainty of ET estimates. While it has been stressed that improvements in the estimation of G and  $Q_s$  are very important for energy closure (Heusinkveld et al., 2004; Myers and Hollinger, 2004), the importance of biomass storage terms in resolving diurnal energy imbalance has sometimes been downplayed regarding the energy closure problem (Foken, 2008; Hendricks Franssen et al., 2010). Given the complexity of 3-dimensional above-ground biomass and development of instrumentation and methods for measurement, quantification of  $Q_s$ ,  $Q_A$ , and G are more practical than measuring  $Q_B$ . Varying quantity and distribution of leaves, tree stems, coarse woody debris (CWD), and fine litter act as insulation between the atmosphere and soil, reducing the amount of heat that would otherwise penetrate the soil surface affecting  $Q_s$  and G. Therefore, it is equally important theoretically to consider  $Q_B$  alongside  $Q_s$ ,  $Q_A$ , and G, as higher  $Q_B$  at a particular site theoretically leads to decreasing amplitude and phase of  $Q_s$  and G, changing the relative importance of storage sinks. Thus, for forested sites with significant vertical temperature gradients within the canopy,  $Q_B$  is particularly important. Therefore, the role of heat storage terms in the energy

balance in the fetch of eddy covariance sensors at Hawaiian montane rainforest sites addressed in this thesis needs to be evaluated to improve the sub-hourly energy budget and resolve the diurnal pattern of energy fluxes.

Biomass heat storage is a term that has been previously neglected or simplified in energy balance calculations because mean daily values rarely exceed  $2\text{--}3 \text{ W m}^{-2}$  (Wilson and Baldocchi, 2000), and its quantification is made difficult by the complexity of different vegetation covers. However, some studies report that the relative contribution of  $Q_B$  can be significant during the night and in the morning hours and for conditions like overcast days or immediately after rainfall (McCaughey, 1985), and reach maximum values on the order of  $60 \text{ W m}^{-2}$ . Measurements of  $Q_B$  are increasingly considered essential at eddy covariance sites due to high values of  $80 \text{ W m}^{-2}$  reported in Amazon forest by Moore and Fisch (1986). More recently, Michiles and Gielow (2008) reported that on average, above ground biomass and air heat storage during midday was 15% of  $R_{NET}$ , and was 65% of  $R_{NET}$  before sunrise. Silberstein et al. (2001) measured similarly high early morning contributions of storage of up to 69% of  $R_{NET}$  in a native jarrah (*Eucalyptus marginata*). Kobayashi et al. (2012), used a 3-dimensional modeling approach in a woody oak savannah in California, USA, and found that 12% of the daytime energy flux was used for heat storage of stems. McCaughey and Saxton (1988) noted that each of the storage terms contributed significantly to the energy balance for differing environmental conditions and time of day.

As mentioned above, several authors have suggested improved  $\Omega$  when  $Q_B$  is measured compared to if it is neglected. This would be theoretically expected because negative night-time values of available energy would be increased closer to zero when heat release by the vegetation is taken into account, and positive daytime values of available energy would decrease due to heat absorption, increasing  $\Omega$ . Also, it is possible that including heat storage terms in the energy balance will reduce the coefficient of determination ( $r^2$ ) of the regression between available energy and turbulent fluxes because it is expected to improve alignment for each 30-minute energy budget. Inclusion of carefully estimated  $Q_B$  into the energy balance has improved energy balance closure by up to 10% (Michiles and Gielow, 2008), and at a few sites energy closure was resolved within 5% with inclusion of  $Q_B$  and  $Q_A$  (Lamaud et al., 2001; Meyers and Hollinger, 2004; Haverd et al., 2007; Jacobs et al., 2008; Moderow et al., 2009; Lindroth et al., 2010). Oliphant et al. (2004) did not report the difference in energy closure when  $Q_B$  was measured in a temperate deciduous forest. However it was noted that G dominated seasonal

variation in combined soil, air, and biomass heat storage fluxes ( $Q_{SUM}$ ,  $W m^{-2}$ ) while other heat storage sinks were more important on a diurnal basis. Wilson et al. (2002) found that on average, energy closure improved 7% when  $Q_B$  was included in the energy balance for forested sites. However many of these sites still exhibited large energy imbalances, and it has been concluded that  $Q_B$  is an important component in tall canopies, but not necessarily the sole source of the lack of energy closure among sites (Aubinet, 2008; Moderow et al., 2009).

Another method to determine energy closure widely reported in energy balance studies is the bulk energy balance ratio (EBR) method, which can be evaluated as the sum of the absolute LE and H values divided by the sum of the available energy over a given time period. In the context of heat storage, it is important to describe the limited capacity of this method to resolve the energy balance properly. Heat storage terms ( $G$ ,  $Q_A$ , and  $Q_B$ ) contribute very little to the energy balance closure over the long term since they are nearly balanced over a 24 hour period (Mahrt, 1998), and error cannot be quantitatively evaluated. Because diurnal variations in heat storage terms are not accounted for using the EBR method, and noting spurious results at some sites when EBR was evaluated in Wilson et al. (2002), its use in resolving the site specific energy balance is limited. Evaluating  $\Omega$  is more useful for this purpose because energy closure can be theoretically improved with inclusion of heat storage terms by shifting individual points in the regression closer to 1:1. Assessment of  $\Omega$  on a sub-hourly basis takes into account important periods of the day when tall canopies have the potential to absorb and release a significant portion of the available energy if all heated elements are taken into account.

An adjustment that is often applied to flux measurements is to divide LE and H by  $\Omega$  or by the EBR (Fischer et al., 2009; Giambelluca et al., 2009; Kume et al., 2011). What that does is “correct” the turbulent fluxes to achieve energy closure by proportionally changing LE and H such that the Bowen ratio ( $H/LE$ ) is not changed (Twine et al., 2000). This adjustment is justified by assuming the energy deficit is due to systematic biases in eddy covariance measurements such as failure to resolve low frequency fluxes from large eddies when averaging the mean fluctuations over 10 Hz intervals, or sloping terrain that induces nocturnal drainage. In effect, daytime heating decreases the relative amount of available radiation that would otherwise be assumed to drive H and LE, and ET may be overcorrected if energy storage terms are neglected or not properly measured. Also, energy storage terms that are not modeled at the same time interval as the turbulent fluxes may result in misleading values of  $\Omega$ , i.e. if the mean diurnal cycle of energy storage terms in the energy balance are used (Giambelluca et al., 2009). Using  $\Omega$  to

adjust LE and H upward based on lack of closure is suggested due to the above reasons, and while acknowledging both  $\Omega$  and EBR methods have limitations,  $\Omega$  is an improvement to EBR when evaluating energy closure at a specific site because it corrects energy closure on a diurnal basis, and improvement can be expected by including the storage terms at higher time resolution (e.g. 30 min or 1 hr). Recently, theoretical considerations have questioned the validity of using  $\Omega$  to determine overall energy closure (Hendricks Franssen et al., 2010) due to poor night-time energy closure. Based on the limitations of both methods of determining energy closure discussed above, it is reasoned that researchers can increase the quality of energy closure assessments by evaluating the absolute energy imbalance according to particular environmental conditions, including stability parameters, turbulence, and time of day.

#### 1.4 Estimation of Biomass Heat Storage

It is common to determine  $Q_B$  from temperature measurements installed in tree stems, and evaluated for each biomass component as:

$$Q_B = dT_B \times B_S \times C_B \quad [3]$$

where  $dT_B$  is the temperature change from the previous to the current time-step for each component of fresh biomass ( $B_S$ ,  $\text{kg m}^{-2}$ ), and  $C_B$  ( $\text{J kg}^{-1} \text{ }^\circ\text{C}^{-1}$ ) is the specific heat of each biomass component. The total fresh biomass at each site ( $B_F$ ,  $\text{kg m}^{-2}$ ) is the sum of all components  $B_S$  integrated over the surveyed area. Differential rates of heating of insulated and exposed portions of biomass complicates the process of scaling temperature measurements in a few locations to the stand level, as scaling up requires determination of the proportion of the biomass that is best represented by the location of the temperature sensors. Thus, evaluation of  $Q_B$  requires plot-level surveys and detailed analysis of site-specific vegetation structural information. Considering the complex distribution of forest canopy elements it is important to quantify the radial distribution of boles and branches, otherwise non-weighted temperature averaging poorly reflect actual biomass temperature measurements. While accurate and precise temperature representation from thermocouple measurements in complex forest environments is nearly unattainable, over-simplification of methodology may lead to ambiguous results.

It is often assumed that  $C_B$  is constant for different biomass components. Reported values of  $C_B$  used in studies of  $Q_B$  range from 2407 (Michiles and Gielow, 2008) to 3340 J kg<sup>-1</sup> °C<sup>-1</sup> (Wilson and Baldocchi, 2000; Wilson et al., 2002). Oliphant et al. (2004) used a constant  $C_B$  value of 2928 J kg<sup>-1</sup> °C<sup>-1</sup> following Thom (1975) and other authors (McCaughey, 1985; McCaughy and Saxton, 1988). Recent detailed studies have compiled site specific estimates of  $C_B$ . Haverd et al. (2007), calculated the mean of values for cellulose and water, weighted by the densities of dry wood and water, and provided a constant value of  $C_B$  at 2760 J kg<sup>-1</sup> °C<sup>-1</sup>. Michiles and Gielow (2008) calculated  $C_B$  as a function of the specific heat of cellulose, the moisture content, and the specific heat of water for each species and tree component, including trunk, branches, twigs, leaves, fine litter, and other small sized vegetation components, and average trunk  $C_B$  was estimated to be lower than previously reported at 2407 J kg<sup>-1</sup> °C<sup>-1</sup>, while leaf  $C_B$  was 2769 J kg<sup>-1</sup> °C<sup>-1</sup>. Despite the assumption by Oliphant et al. (2004) that the sensitivity of total  $Q_B$  to the choice of  $C_B$  is small, according to Equation 7,  $Q_B$  is linearly related to  $C_B$ , and the variation is as much as 30% based on more recent  $C_B$  ranges reported in the literature (2407-3340).

Where it is possible to measure trunk temperatures, screen for data quality, and estimate representative contributions of biomass components, field based estimates of  $Q_B$  carry added credence than that of a parameterized model based on air temperature and the canopy radiation environment. However, due to sampling limitations and for validation of measured values, researchers have devised analytical models for calculating the time-series of heat storage in biomass components independent of trunk temperature (Meesters and Vugts, 1996; Haverd et al., 2007). While these methods require intensive parameterization, Haverd et al., (2007) reported improvement of energy balance closure of 10% and good agreement with measured and modeled trunk temperatures. By comparing results against their own model Haverd et al. (2007) found that the model of Meesters and Vugts (1996) produced a mean mid-day underestimation of  $Q_B$  of 50 W m<sup>-2</sup> which they attributed to neglect of heat transfer by radiation. The model proved to be in good agreement with the two layer Force-Restore method similar to that used in Silberstein et al. (2003). The Meesters and Vugts (1996) model found that a mass weighted mean average trunk radius may be sufficient for the purpose of evaluating biomass energy storage, and the Haverd et al. (2007) model found that the vertical profile of  $Q_B$  may not be absolutely necessary, as output differed by only 5 W m<sup>-2</sup> when multi-layer forcing variables were averaged. Comparison of analytical models with results using actual temperature

measurements has the benefit of showing where simplification may be acceptable, and these models have greatly improved our understanding of  $Q_B$  and its effects on  $\Omega$ .

While species specific biomass regressions exist that relate tree diameter and height to biomass, uncertainties are often high when generalized allometry is used or wood density unknown (Michiles and Gielow, 2008). It is therefore important to incorporate species specific biomass allometry if data are available, although this may not be practical in forests with high diversity and complex structure. However, allometric models are rarely found in the form where radial and vertical biomass distribution can then be evaluated from basic field vegetation surveys. Due to these limitations, it is desirable to have the option of evaluating  $Q_B$  using the models described above, or for some purposes simplification may be a more convenient option using trunk temperature measurements without explicitly accounting for variable radius of canopy tree stems (McCaughey, 1985; Giambelluca et al., 2009). Oliphant et al. (2004) simplified evaluation of energy storage for complex stem distributions by separating biomass and temperature measurements into two components, bole and branch, and placed a limited number of sensors throughout the canopy in 6 trees. Species specific biomass estimates were calculated from general allometric equations of deciduous tree bole and branch biomass. While a suite of simplifications are always necessary to scale up  $Q_B$ , care must be taken to reduce uncertainty in its estimate considering the importance of precision in hydrological applications.

### 1.5 Gap-filling Latent and Sensible Heat Fluxes

A considerable barrier in temporally integrated measurements of gas exchange in wet forests is that the eddy covariance sensors are often impaired by wet sensor surfaces from rain, fog, or dew and functionality is not resumed until the sensors dry out. Additionally, instrumentation is subject to frequent failure in highly humid environments such as those discussed in this study. Montane rainforests that receive most of their precipitation from orographic lifting are particularly prone to large proportions of missing data due to wet sensors, as frequent fog occurrence can extend the down-time of turbulent flux measurements compared to lowland tropical forests that receive similar amounts of total precipitation in characteristically short, heavy downpours. Therefore, accurate long-term ET estimates in frequently wetted ecosystems are reliant upon rigorous filling procedures based on meteorological data. Alavi et al. (2006) investigated the extent of uncertainty in ET estimates due to filling LE with various models, and

found that the Kalman filtering approach with dynamic linear regression worked best, followed by a multiple regression approach. Both of these approaches include input of available radiation, however, in Alavi et al. (2006), above ground heat storage terms were neglected and available energy was given as  $R_{NET} - G$ . It is expected that including  $Q_B$ ,  $Q_A$ , and  $Q_S$  in estimates of available radiation will reduce error in modeled values.

#### 1.6. Related Prior Research

At the research site at Nahuku on Hawai'i Island (section 2.2), one of the two sites discussed in this paper,  $\Omega$  was reported as 0.784 (Giambelluca et al., 2009) for a one year period. At the two tropical montane forest sites in Hawai'i to be discussed in this paper, Nahuku and 'Ōla'a, soil heat flux is only a small fraction of the total heat storage flux.  $Q_B$  was included in Giambelluca et al. (2009) in evaluation of  $\Omega$ , and the effect on  $\Omega$  was small (unpublished data). Giambelluca et al. (2009) used measurements of stem temperature, air temperature and estimates of biomass, and included them in analysis of energy closure. However, since the observation period of stem temperature was short (6 months), the mean diurnal cycle of heat storage was used as the time series and day to day variation was not resolved leading to spurious energy balance corrections for days significantly different than the mean diurnal cycle. The analysis in Giambelluca et al., (2009) also involved significant simplifying assumptions about the vertical and radial distribution of biomass, whereas detailed methods to address estimation of biomass distribution were undertaken in the present study. It is expected that increasing the size of survey plots from previous investigations will improve analysis of biomass distribution, a superior temperature averaging technique will allow the biomass to be better represented by limited temperature measurements, and application of sub-hourly  $Q_B$  time series will lead to more reliable  $\Omega$  evaluations at this site. Furthermore, inclusion of all storage terms will help to constrain the diurnal energy fluxes and reduce error in regressions used to fill LE and H and will allow energy closure to be evaluated based on environmental conditions and time of day.

## CHAPTER 2. METHODS

### 2.1 Overview

In this study,  $Q_B$  is rigorously evaluated at two forested eddy covariance sites in Hawai'i Volcanoes National Park as a means of improving energy closure. Biomass heat storage sinks include canopy tree stems, sub-canopy tree-fern stems, leaves, fine litter, coarse woody debris, and epiphytes. This study makes use of a detailed structural study of 'ōhi' a lehua (*Metrosideros polymorpha*) (Gerrish, 1988), in close proximity to Nahuku (site descriptions in section 2.2), and develops allometric relationships from destructive sampling for strawberry guava (*Psidium cattleianum*), an invasive species at the 'Ōla'a site, in order to quantify the vertical and radial distribution of stems in both of these dominant tree species in Hawaiian wet forests. Trunk temperature measurements are limited to a sample size of 20 sensors in one tree and one tree fern at each site due to instrumentation and canopy access constraints, and were placed on medium sized trees at representative locations. At a 30-minute interval temperature change at each location in the canopy is multiplied by fresh biomass and specific heat corresponding to that location to calculate changes in energy storage (Equation 3). This study examines 34 months (July, 2007 – Feb, 2010) of eddy covariance flux measurements, net radiation, stem and air temperature profiles, and soil heat flux data that were compiled, screened, and processed to evaluate energy closure with and without inclusion of energy storage. At each site, a comparison is done to determine whether inclusion of the heat storage term improves energy closure at these wet forest sites with moderately high biomass. Individual 30-minute values of  $\Omega$  and the mean absolute energy imbalance ( $E_{ABS}$ ) are then grouped in equal sized bins and evaluated in relation to 1) inclusion of various heat storage terms, 2) time of day, 3)  $u^*$ , and 4)  $\xi$ .

### 2.2 Site Descriptions

Site descriptions are documented in Giambelluca et al., (2009) at Nahuku (19°24'55" N, 155°14'18" W), and Takahashi et al. (2011) at both Nahuku and 'Ōla'a (19°28'43" N, 155°12'47" W), and they are elaborated on here in the context of canopy structure, an important parameter when quantifying  $Q_B$ . The dominant native species in Hawaiian forests is *M. polymorpha*, a

species that is able to pioneer newly formed volcanic substrate. In wet forests, after the 'ōhi' a canopy closes, a broad array of indigenous and endemic flora and fauna are provided suitable microclimatic and nutrient conditions to nourish evolving Hawaiian ecosystems. Unlike tropical forests in continental environments, Hawai'i has much lower plant species diversity, reducing the structural heterogeneity of native forests compared to continental tropical and subtropical forests. Native ecosystems are extremely prone to invasion due to their evolution in isolation with limited competition, and species invasions can rapidly change the structure and functioning of Hawaiian ecosystems (Vitousek, 1990; Asner et al., 2008).

At Nahuku, the native Hawaiian forest has been restored by removing invasive plants and fencing out and eradicating invasive animals. The substrate age is 222 years old, formed by the eruption of Kilauea in 1790. Mean annual rainfall measured from the flux tower from 2007–2009 was  $2532 \pm 324$  mm yr<sup>-1</sup> and elevation is 1200 m (19°24'54.80"N, 155°14'18.41"W). For trees greater than 5 cm diameter at breast height ( $D_{BH} = 1.3$  m), *M. polymorpha* represents 90 % of the total basal area and *Ilex anomala* represents 10 % with average canopy height about 17 m. *Cibotium* spp. tree ferns inhabit a sub-canopy layer and reach 3–5 m in height. A diverse array of understory trees and shrubs give an indication of the increasing diversity that can be expected as this stand ages and the original *M. polymorpha* canopy begins to die out. A thick recalcitrant layer of leaf litter covers the forest floor at this site, mostly consisting of slowly decaying *M. polymorpha* leaves and *Cibotium* spp. fronds.

At the 'Ōla'a station 7.5 km to the NNE at 1043 m (19°28'42.66"N, 155°12'54.01"W) the mean annual rainfall measured from the flux tower was  $3220 \pm 370$  mm yr<sup>-1</sup> from 2007–2009. Here, forest structure is complicated by a higher diversity of trees and a patchy forest development. The older 3,000–5,000 year-old substrate at 'Ōla'a (Wolfe and Morris, 1996) has provided more time for soil and forest development, and natural succession and has led to a more diverse ecosystem with a patchier landscape and higher proportion of tree ferns and other canopy species. Tree species such as *Ilex anomala* and *Cheiropendron trigynum* germinate in the light environment provided by the *M. polymorpha* canopy, allowing a more diverse canopy on older substrates in these native Hawaiian forests. Additionally, dieback of *M. polymorpha* at 'Ōla'a has led to displacement by *Cibotium* spp. (Mueller-Dombois et al., 1977). The 'Ōla'a site has been heavily invaded by *P. cattleianum*, a highly invasive plant that threatens to destroy native ecosystems (Smith, 1985) and negatively impact hydrological functioning of native Hawaiian forests (Giambelluca et al., 2007).

### 2.3 Meteorological Measurements

At Nahuku and 'Ōla'a, meteorological towers (18 m and 25 m, respectively) were erected and instrumented with eddy covariance systems described in Giambelluca et al. (2009). Frequent and sustained periods of rain and fog regularly wetted the sonic anemometers (model CSAT3, Campbell Scientific, Logan, UT, USA) and open-path infrared gas analyzers (model LI-7500, Licor, Lincoln, NE, USA), and caused significant loss of data as these sensors do not function properly when wet. Only 35.5% and 40.7% of LE and H were available after screening for wet sensor periods at Nahuku and 'Ōla'a, respectively. However instrument calibrations, long term maintenance and manual and systematic data screening procedures were implemented so as to maximize data availability. Eddy covariance data stored at 10 Hz was processed to determine H and LE according to Giambelluca et al. (2009) at 30 minute intervals. While both eddy covariance systems have been in operation for more than 5 years, the period for this study (May, 2007 to Feb, 2010) was chosen because it was the period with the least amount of missing data necessary to determine  $Q_B$  and  $Q_A$ , including  $R_{NET}$ ,  $G$ ,  $Q_S$ , stem temperature ( $T_S$ , °C), air temperature, and relative humidity (model HMP45C, Vaisala, Helsinki, Finland). Net radiation was measured with a high-standard four component radiation sensor (model CNR1, Kipp and Zonen, Delft, The Netherlands) at both sites for the period of this study and sensors were calibrated at two-year intervals according to manufacturer recommendations. Stem temperatures were measured with thermocouple sensors at three heights in one tree, with four sensors located azimuthally around the stem and a deeper sensor installed in tight-fitting holes drilled into the stem (TT-T-24-SLE, thermocouples fabricated from Omega Engineering (Stamford, CT, USA) thermocouple wire,). The 50 cm of thermocouple wire nearest the sensing junction was wrapped in reflective tape to minimize the effect of heat conduction on the measurements. At Nahuku, a medium sized *M. polymorpha* tree ( $D_{BH} = 20$  cm) was outfitted with  $T_S$  sensors at 3, 9, and 15 m, while at 'Ōla'a, a medium-sized *P. cattleianum* tree ( $D_{BH} = 8$  cm) was used to measure  $T_S$  at 3, 5, and 7 m. Additionally  $T_S$  was measured similarly in 1 tree fern stem at each site at 0.5 m height, with four outer sensors placed azimuthally at 1.5 cm depth and a deeper sensor at 5 cm. Since no temperature sensors were placed in leaves, epiphytes, litter, and dead wood, proximal stem or air temperature sensors were assumed to represent the temperature of these components. Leaf and epiphyte temperatures are assumed to be represented by shielded air temperature thermocouple measurements (3, 9, and 15 m at

Nahuku; 3, 5, and 7 m at 'Ōla'a), litter temperature is assumed to be represented by tree fern temperature at 1.5 cm depth, and CWD temperature is assumed to be represented by inner and outer tree fern temperature for its inner and outer portions, respectively. Four soil heat flux plates (model HFT-3, Radiation and Energy Balance Systems, Seattle, WA, USA) were installed at 8 cm below the bottom of the organic horizon to measure G, and two 4-probe averaging soil temperature sensors and one soil moisture reflectometer (CS-616, Campbell Scientific) were used to measure  $Q_s$  for each 30 minute period. At each site, data were stored at 30-min intervals by two dataloggers (models CR5000 and CR1000, Campbell Scientific), while data necessary for turbulent flux calculations were stored at 10 Hz.

## 2.4 Survey Plots

Detailed surveys upwind of meteorological towers at Nahuku and 'Ōla'a plots were conducted in eight and six 100 m<sup>2</sup> plots, respectively, between 2004 and 2007, in correspondence with vegetation surveys in throughfall and stemflow plots (Takahashi et al., 2011), epiphyte and biomass water storage capacity surveys (Mudd, 2004; Mudd and Giambelluca, 2006), and carbon inventory plots (unpublished data). All data from biomass plots collected at these sites were combined to obtain the best possible representation of field biomass. Although based on a relatively small sample (600-800 m<sup>2</sup>) due to time and labor limitations involved in field surveys, these highly-detailed survey data were sufficient to estimate plot and stand level biomass at the two sites. Table 2.1 describes vegetation characteristics and plot level variability of biomass in the surveys.

In each survey plot,  $D_{BH}$  was measured for all trees greater than 5 cm  $D_{BH}$ , and the species of each tree was identified. All tree fern stems (*Cibotium* spp. and *Sadleria* spp.) were measured at the midpoint height of the caudex. Supplemental surveys of *P. cattleianum* individuals within the 2–5 cm range was undertaken within 2 of 6 plots at the 'Ōla'a site, and extrapolated to the stand. Numerous smaller *P. cattleianum* individuals make up an unusually high proportion of the total biomass at 'Ōla'a. All other trees and shrubs with  $D_{BH}$  less than 5 cm at both sites appeared to represent an insignificant proportion of the biomass, and they were neglected in the surveys. For some individuals, the frond radius was also measured. Coarse woody debris was measured within four 20-m<sup>2</sup> subplots at each site by measuring the length

and diameter of all snags and fallen stems >2.5 cm diameter. Accumulated fine litter was collected from twelve 0.25 m<sup>2</sup> randomly-placed sub-plots at each site, weighed, and extrapolated to the survey area. Epiphyte biomass was determined from surveys conducted by Mudd (2004) within the same survey plots.

## 2.5 Determination of Total Biomass -Allometric Models

Total aboveground dry stem and leaf biomass for *M. polymorpha* ( $B_{T\_MP}$ ) was determined from a species specific allometric equation (Mascaro et al., 2011; model 1) relating  $D_{BH}$  (cm) to plant dry biomass (g) as ( $n = 30$ ;  $D_{BH}$  range: 0.3–33.1;  $r^2 = 0.74$ ):

$$B_{T\_MP} = 0.2957 \times (D_{BH})^{2.0941} \times 1.1752 \quad [4]$$

Stem dry biomass was determined as the difference between  $B_{T\_MP}$  and leaf dry biomass ( $B_{L\_MP}$ , kg), calculated from Litton and Kauffman (2008) as ( $n = 30$ ;  $D_{BH}$  range: 0.3–33.3 cm;  $r^2 = 0.94$ ):

$$B_{L\_MP} = 0.09 \times (D_{BH})^{2.25} \quad [5]$$

While several allometric models for *M. polymorpha* based mostly the same harvest data (Raich et al., 1997; Litton and Kauffman, 2008; Asner et al., 2011) are available, an assessment conducted by Mascaro et al. (2011) showed that linear models that incorporated the full range of harvested trees fit to log-transformed diameter and biomass data were the most appropriate. It is expected that because several of the trees used in the allometric models were taken from nearby Nahuku, species specific biomass allometric regressions between diameter at 1.3 m and biomass is expected to produce more accurate results of  $Q_B$  than would an alternative non-species specific model i.e., that of Chave et al. (2005); a commonly used model developed mostly from trees found in the continental tropics.

To determine the biomass of *Cibotium* spp., stem volume of all individuals were calculated from survey data, and an allometric model (Arcand et al., 2008) was used to scale up leaf area based on frond radius at Nahuku. Frond radius of tree ferns was not measured in the 'Ōla'a survey, so caudex height was used as a predictor for frond biomass prediction for this site.

Allometric models for *I. anomala* and *C. trigynum* (Raich et al., 1997) do not include any individuals greater than 10 cm  $D_{BH}$ , and thus cannot be reasonably extrapolated to the size range of trees at the study sites. For these tree species, the *M. polymorpha* model was used. To correct for differential wood density, modeled biomass was multiplied by the ratio of *I. anomala* and *C. trigynum* wood density to *M. polymorpha* wood density. For *I. anomala*, using the same model as *M. polymorpha* is quite reasonable as the species are similar in growth form, and its contribution to the total biomass is small. Because *C. trigynum* is somewhat abundant at 'Ōla'a, representing 14.3 % of the basal area of canopy tree species (not including tree ferns), and is different in form and structure compared to *M. polymorpha*, using the allometry equation for *M. polymorpha* to predict biomass of this species is subject to error. Also, because each olapa is so different, it would be difficult to be confident of any allometric equation applied. However, it was decided to use the *M. polymorpha* model to predict biomass of *C. trigynum* for lack of better options. To scale *P. cattleianum* biomass to the stand level, five trees were destructively harvested and allometric models were created to determine the vertical and radial distribution of biomass in each of 4 stem compartments. See section 2.6 for a description of the methodology used to determine the vertical and radial distribution of biomass at each site.

While stem growth of *P. cattleianum* may have been significant during the period between the survey and biomass estimates, and the Nahuku forest appears to be slowly growing as well, biomass is assumed constant with time. It was assumed that this error is small and difficult to determine, considering incorporation of a growth function would need to be supplemented by mortality and turnover, data that is currently non-existent for transitional natural forests being invaded.

To convert measured volume of  $Q_B$  components to  $B_S$  (including water), component-specific wet density was used. To convert dry wood and leaf biomass determined from allometric equations to field fresh biomass, dry-to-wet ratios described by Aplet and Vitousek (1994) were utilized. While the wet density of forest elements such as CWD (also litter, epiphytes, and porous tree fern stems) are spatially and temporally heterogeneous at a particular site due to their high water storage and frequent wetting and drying cycles, varying water storage of these elements is difficult to measure. In a sub-alpine dark coniferous ecosystem on the Qinghai-Tibetan Plateau in China, Yu et al., (2004) found that as CWD decays and dry wood density decreases, wood moisture content increases because more pore space is available for water to infiltrate. Thus it is assumed that fresh density of CWD remains

approximately the same regardless of decay class, and constant values of fresh density are assumed. Following Table 3 in Yu et al. (2004), fresh density (the product of the relative water content and the wood density under natural conditions) for 5 decay classes was found to range between 0.97 and 1.03 g cm<sup>-3</sup> for fallen trees, and between 0.75 and 0.87 g cm<sup>-3</sup> for snags. The initial dry wood density of the class with little or no visible decay for CWD in Yu et al. (2004) was 0.48 g cm<sup>-3</sup>, lower than that of *M. polymorpha* (0.69 g cm<sup>-3</sup>) which makes up the majority of CWD at both study sites. Thus, it was assumed that without further knowledge, a value of 1 g cm<sup>-3</sup> for CWD was a fair approximation of fresh density of CWD at the study sites, and this value was used for all CWD originating from canopy trees. Because the wood density of *Cibotium* spp. (mostly *Cibotium glaucum*) is much lower than that of *M. polymorpha* (Table 2.2), the fresh density of dead *Cibotium* spp. stems was assumed to be lower than that of CWD originating from canopy trees, and the same value as live *Cibotium* spp. stems was used for *Cibotium* spp. CWD (0.60 g cm<sup>-3</sup>). Due to the relatively new ecosystem development at Nahuku, CWD mostly consists of snags, with fallen trees very rare. Therefore, at Nahuku CWD is not considered to be as an important factor as at 'Ōla'a. At 'Ōla'a, where mature *M. polymorpha* trees experience occasional mortality, CWD is expected to be large with high spatial variability. While the limited measurements of CWD in the survey plots give an approximation, they may not be fully representative of the stand.

## 2.6 Vertical and Radial Distribution of Stem Biomass

### 2.6.1 *Metrosideros polymorpha* and Other Native Trees

Since vertical and radial stem temperature gradients are evident in skin temperature data at the study sites, especially in large diameter stems, it is necessary to make separate estimates of heat storage in biomass components differentiated by depth within the stem and height above the ground. To do so requires temperature measurements in representative locations with each biomass compartment and determination of the biomass represented by each temperature sensor. From here on in this thesis, 'compartment' will be used to refer to a section of a stem (i.e. the annular portion of biomass from 0-4 m), and 'component' will be used to differentiate different types of biomass (i.e. native tree stems, foliage, litter, etc.) To estimate the vertical and radial distribution of the biomass of the dominant species in detailed field survey plots (*M.*

*polymorpha*), existing raw data for trees harvested in close proximity to Nahuku were used (Gerrish, 1988). Based on harvest data, Gerrish (1988) constructed a figure of an average mature *M. polymorpha* tree drawn to scale, including main stems and branches greater than 2 cm diameter. Acknowledging the limited resolution of the figure, it was determined that this was the best available information on the vertical and radial distribution of stem biomass for *M. polymorpha*. The figure was enlarged, stratified into 16 vertical sections, and the length and midpoint diameter of each section within each vertical stratum were measured (Figure 2.1a). The volume of each measured section was calculated assuming a cylindrical shape. From these measurements a vertical biomass profile was constructed, relating the percent of total tree volume in each stratum to the ratio of total tree height (Figure 2.1b), assuming all native trees exhibit the same proportional structure predicted by measured  $D_{BH}$ .

The distributions of main stem and branch volumes of all trees in the survey plots were calculated separately for six compartments (core and skin volume for each of three vertical stem sections) for all measured trees according to the proportions measured in Figure 2.1a. The estimated total tree height ( $Ht_{TREE}$ , m) of each tree in the survey plot is given in Asner et al. (2009) as ( $n = 96$ ;  $r^2 = 0.87$ ):

$$Ht_{TREE} = 5.67 \times \ln(D_{BH}) - 4.041 \quad [6]$$

The length of each stem section for trees in the survey plot ( $L_{STEM}$ ) is calculated based on the proportions measured in the enlarged Figure 2.1a as:

$$L_{STEM} = Ht_{TREE} \times \frac{L_M}{Ht_{FIG}} \quad [7]$$

where  $L_M$  is the length of the measured stem in the enlarged Figure 2.1a and  $Ht_{FIG}$  is the total measured height of the tree in the enlarged Figure 2.1a. The radius of each stem section for trees in the survey plot ( $R_1$ , cm) is given as:

$$R_1 = \frac{1}{2} \frac{D_M}{D_{BH\_FIG}} \times D_{BH} \quad [8]$$

where  $D_M$  (cm) is the measured diameter at the midpoint height of each section in each stratum measured from the enlarged Figure 2.1a, and  $D_{BH\_FIG}$  (cm) is the measured  $D_{BH}$  of the enlarged Figure 2.1a.

All stems were divided into an outer annulus (skin) and an inner cylinder (core). The temperature measurement of the skin ( $T_{SKIN}$ ) is positioned at the center of mass of the annular volume ( $V_{SKIN}$ ,  $cm^3$ ) with radius  $R_{T1}$  (cm), and is calculated as the four sensor average temperature each 30-minute interval. The outer temperature sensors are installed at depth  $zT_S$  (four sensors at 1 cm depth in trees and 1.5 cm depth in tree ferns) and are located between the surface of the stem at radius  $R_1$  and the boundary between  $V_{SKIN}$  and the volume of the inner cylinder ( $V_{CORE}$ ,  $cm^3$ ) with radius  $R_2$  (cm) given as:

$$R_2 = \sqrt{2(R_1 - zT_S)^2 - R_1^2} \quad [9]$$

and

$$V_{CORE} = \pi R_2^2 L \quad [10]$$

$V_{SKIN}$  is calculated as the difference between the total stem volume ( $V_{TOTAL}$ ,  $cm^3$ ) and  $V_{CORE}$ , where

$$V_{TOTAL} = \pi R_1^2 L \quad [11]$$

and

$$V_{SKIN} = V_{TOTAL} - V_{CORE} \quad [12]$$

The core volume is dependent on the depth of outer stem temperature measurements and the size of the stem. Figure 2.2 illustrates the variables used in geometric separation of biomass. From Equation 9, the minimum diameter of a stem with a core volume is 6.8 cm and 10.2 cm (with  $zT_S$  at 1 cm and 1.5 cm, respectively), otherwise stem sections smaller than this are assumed to be represented by  $T_S$  only (i.e. with a core volume of zero).

After tree biomass was separated into the 16 vertical strata for each tree, all trees in the survey plots were then combined into three vertical sections based on the height of stem

temperature measurements (Section 2.7). The vertical sections were defined to be 0–6 m, 6–12 m, and 12–20 m at Nahuku and 0–4 m, 4–6 m, and 6–16 m at 'Ōla'a. To divide the 2 layered stems (skin and core) into 3 vertical sections corresponding to the height of temperature measurements based on the 16 strata shown in Figure 1a for each tree in the survey plot, the height of the bottom ( $Ht_{i,j}$ , m) and top ( $Ht_{i,j}$ , m) of each stratum was calculated as:

$$Ht_{i,j} = Ht_{TREE} \times \frac{Ht_{FIG\ i,j}}{Ht_{FIG}} \quad [13]$$

To calculate stem volume in the appropriate vertical height ranges when any of the 16 strata exist in more than 1 height range (i.e. if the seventh strata on a particular tree at either site ranges from 5.7–6.4 m height), the volume of each section was multiplied by the proportion of height of each section located within each height range.

Because Fig 2.1a only includes the main stem and branches, twig dry biomass ( $B_{TW}$ , g) was estimated based on measurements of stems of 5 harvested mature *M. polymorpha* individuals (Gerrish, 1988) for stems less than 2 cm diameter. Linear regression yielded the following relationship between  $D_{BH}$  and  $B_{TW}$  for *M. polymorpha* ( $n = 5$ ; DBH range: 14.4–28.8;  $r^2 = 0.59$ ):

$$B_{TW} = 172D_{BH} + 432.5 \quad [14]$$

Inputs to estimate twig volume for each tree in the survey area are  $B_{TW}$ ,  $Ht_{TREE}$ , and the 3 height ranges at each site for each tree in the survey area and the relative height where twigs are located on each tree. It was observed from Figure 2.1a that the distal ends of branches were all located above 68% of the relative tree height, and that all twigs occur at the two uppermost height ranges for all trees at both sites. For simplification, it is reasonable to assume twig biomass density above 68% of tree height is constant.  $B_{TW}$  for each height range was determined as the product of total  $B_{TW}$  and the proportion of  $B_{TW}$  located in each height range.

To test the prediction of *M. polymorpha* biomass using the method described above, the estimated total volume of each tree in the survey area at Nahuku was multiplied by dry wood density, and plotted against biomass derived from Mascaro et al., (2011), and Asner et al. (2011) (Figure 2.3). On a stand level basis, the model described above indicated 22% higher biomass compared to Mascaro et al. (2011), and 9% lower than Asner et al. (2011). To align stem

biomass with the allometric equation for *M. polymorpha* (Mascaro et al., 2011), the total volume determined in each of the six stem compartments (skin and core for 3 height ranges) was converted to a ratio of biomass found within each of those compartments, and multiplied by the total fresh biomass predicted using the Mascaro et al. (2011) allometric equation and field wet-to-dry mass ratio's ( $R_{WD}$ ) of stem and leaf biomass. in Table 2.2, resulting in a corrected estimation of total biomass of native trees in each of three height ranges at two depths.

Modeling of reference stem core temperature ( $T_{MC}$ , °C) at the center of mass of  $V_{CORE}$  at radius  $R_{T2}$  (cm) and depth  $zT_{MC}$  (cm) is described below for *M. polymorpha* and *P. cattleianum* (Section 2.7). For each section of stem,  $zT_{MC}$  is defined as the distance from the surface to  $R_{T2}$ , where

$$R_{T2} = \frac{R_2}{\sqrt{2}} \quad [15]$$

and

$$zT_{MC} = R_1 - R_{T2} \quad [16]$$

The mass weighted average of  $zT_{MC}$  for all sections of stems on all trees in each of the three vertical height zones is used to define  $zT_{MC}$  for each height range corresponding to respective temperature sensors. All *Cibotium* spp. stem and CWD biomass resides in the lowest vertical layer (0–6 m at Nahuku and 0–4 m at 'Ōla'a) so it was not necessary to vertically separate the biomass. For these compartments, radial distribution of biomass and  $zT_{MC}$  were calculated using Equations 8–12, 15, and 16.

### 2.6.2 *Psidium cattleianum*

While results were recently published regarding allometric equations for *P. cattleianum* (Mascaro et al., 2011), no information exists on the vertical and radial distribution of biomass for this invasive species at 'Ōla'a. Five trees were harvested for allometric analysis that encompassed the range of stem diameters measure in field surveys ( $D_{BH}$  = 3.9, 5.6, 6.9, 7.8 and 11.6 cm). Stems smaller than 6.8 cm diameter (the minimum diameter of a stem with a core

volume) were weighed and the diameters at each end and the length were measured. For the harvested *P. cattleianum* stems,  $V_{SKIN}$  and  $V_{CORE}$  were separated using Equations 8 to 12, with the equation for the volume of a cylinder replaced with the equation for the volume of a truncated cone. Above 6 m, all harvested stems were smaller than 6.8 cm diameter.  $V_{CORE}$  from 4 – 6 m only represented 1.2% of the biomass of the largest tree harvested with 11.6 cm  $D_{BH}$ , so core compartments in *P. cattleianum* above 4 m were neglected, limiting separation of *P. cattleianum* to 4 compartments (0–4 m skin, 0–4 m core, 4–6 m skin, and above 6 m skin). Stems measured were converted to fresh biomass using the fresh density, and added to stems that were weighed.

The  $D_{BH}$  of each harvested tree was plotted against the biomass of each of the above mentioned 4 compartments, and the type of regression was chosen as to maximize  $r^2$ . Table 2.3 describes regressions used to predict the biomass in each of the 4 compartments for the surveyed area. Figure 2.4 shows the relationship between  $D_{BH}$  and dry biomass for all harvested *P. cattleianum* trees in this study and similar sized trees harvested by Mascaro et al. (2011). From these data, it can be seen that biomass data from this study are comparable to Mascaro et al. (2011), which harvested trees from another site in windward Hawai'i.

To estimate the mass weighted average of  $zT_{MC}$  in the survey plots for the 0–4 m core compartment in *P. cattleianum* stems,  $zT_{MC}$  was calculated following Equation 16. Linear regression predicting  $zT_{MC}$  from  $D_{BH}$  for this compartment resulted in the formula ( $n = 5$ ,  $D_{BH}$  range: 5.6–11.6,  $r^2 = 0.53$ ):

$$zT_{MC} = 0.039D_{BH} + 2.88 \quad [17]$$

Equations 16 and 17 were applied to all trees in the survey plots that were determined to be large enough to have a  $V_{CORE}$ , and the mass weighted average  $zT_{MC}$  was used to represent the depth of the modeled inner temperature measurement for *P. cattleianum*. While the coefficient of determination of the linear regression in Equation 17 is rather low, it was presumed that this error was insignificant to the final result because the 0–4 m core compartment only represented 2% of the total *P. cattleianum* stem biomass estimated from field surveys, and the great majority of *P. cattleianum* stems were assumed to be well represented by  $T_s$  measurements at 1 cm depth.

An allometric equation for leaf mass of *P. cattleianum* ( $B_{L\_PC}$ , g) was obtained from Flint Hughes (Institute of Pacific Islands Forestry, USDA Forest Service, Hilo, unpublished data) given as ( $n = 26$ ,  $D_{BH}$  range: 0.2–18.2 cm,  $r^2 = 0.95$ ):

$$B_{L\_PC} = 27.914D_{BH}^{2.153} \quad [18]$$

## 2.7 Modeling Stem Core Temperature

Temperature measurements were modeled at the point that represents the mass weighted stand average  $z_{T_{MC}}$  of each tree in the plots. To predict the temperature at  $z_{T_{MC}}$ , the process of sensible heat conduction into and out of wood was simplified assuming a flat surface. Strictly speaking, the conduction of heat into the stems should be considered as occurring in radial direction through the surface area of a cylinder following methods described by Michiles and Gielow (2008) and Moore and Fisch (1986). However, at least 3 measurement depths at each measurement height are necessary to solve the equation for radial heat conduction. Many studies, including this one, have limited measurements of stem temperature at only 1 or two depths (Moore and Fisch, 1986; McCaughey and Saxton, 1988; Silberstein et al., 2001; Oliphant et al., 2004). While determining thermal diffusion in tree stems using the equation designed for heat diffusion through a flat surface is not ideal, Haverd et al. (2007) found good agreement between their analytical method that considers heat diffusion into a cylinder and heat diffusion into the stem modeled analogously to the method used for soil. This method was also applied in the modeling exercise of Silberstein et al. (2003), who used measurements at two depths to solve for the temperature at a given stem radius.

The thermal diffusivity ( $\alpha$ ) is determined from the diurnal average temperature range from sensors at depth  $z_{T_1}$  ( $TR_1$ , °C), and a deeper thermocouple sensor at variable depth  $z_{T_2}$  ( $TR_2$ , °C) as:

$$\alpha = \frac{\pi}{p \left( \frac{\ln \frac{TR_2}{TR_1}}{(z_{T_1} - z_{T_2})} \right)^2} \quad [19]$$

where  $p$  is the period of oscillation (84,000 seconds for a diurnal cycle) and  $zT_1$  and  $zT_2$  are in meters. Calculation of  $\alpha$  in this manner assumes that the ratio of temperature change is constant through the whole stem as determined by two depths. The average diurnal temperature range at  $zT_{MC}$  ( $TR_{MC}$ , °C) is calculated as:

$$TR_{MC} = TR_2 e^{(z_{TC} - z_{TS})} \sqrt{\frac{\pi}{\alpha p}} \quad [20]$$

The temperature anomaly ( $T_A$ , °C) at  $zT_{MC}$  is the estimated temperature difference between each 30 minute interval at depth  $zT_{MC}$ , modeled as:

$$T_A = \frac{TR_2}{TR_{MC}} \times (T_S - \bar{T}_S) \quad [21]$$

where  $\bar{T}_S$  is the mean  $T_S$  for the entire period of analysis. The time lag of the temperature per separation distance between  $T_S$  and  $T_{CM}$  (lag, min cm<sup>-1</sup>) is determined as the time offset associated with the maximum  $r^2$  of the regression between the diurnal cycle of  $T_S$  and  $T_C$ , divided by the difference between  $zT_C$  and  $zT_S$ . After applying the lag, the temperature change for each 30 minute interval at  $zT_{MC}$  ( $dT_{MC}$ ) is the difference between the mean of the current and previous time intervals.  $dT_{MC}$  was calculated separately for each of three height ranges for *M. polymorpha*, *P. cattleianum*, *Cibotium* spp. As stem temperature was only measured in *P. cattleianum* and *Cibotium* spp. at 'Ōla'a,  $T_{SKIN}$  measurements in guava were assumed to represent  $T_{SKIN}$  of *M. polymorpha* (1 cm depth). However,  $\alpha$  derived from *M. polymorpha* measurements at Nahuku were applied to *M. polymorpha* at 'Ōla'a. It must be acknowledged that measurements in the guava stem are not necessarily representative of stem temperature in other species found at the site, and differences in stem diameter and stem surface albedo may influence results. However, canopy access and limited differential channels available in the datalogger prevented a more detailed analysis of  $T_S$ .

## 2.8 Vertical Distribution of Leaves and Epiphytes

To vertically separate leaf biomass predicted by allometric equations described above, the same method described for *M. polymorpha* twigs was used for all canopy tree species at both sites, assuming that the vertical distribution of leaves above 68% of tree height is constant and that all canopy tree species followed this presumed structural behavior. All *Cibotium* spp. fronds at Nahuku are located below 6 m, and thus were all included in the 0–6 m height range. Based on visual observations from the flux tower at 'Ōla'a, it was presumed a reasonable estimate that frond biomass is evenly distributed between the 0–4 m and 4–6 m height ranges. Vertical distribution of epiphyte biomass at the two sites was obtained from a survey of all epiphytes at the same sites in a 20 x 20 m survey at Nahuku, and a 20 x 10 m survey at 'Ōla'a (Mudd, 2004). The survey data was used to extrapolate laboratory measurements of biomass and water storage capacity to the study plot. The biomass was based on the mass when the epiphytes used for laboratory analysis of water content were harvested from the field, and was separated into 3 height ranges discussed above according to the location of the vertical profile of air temperature measurements at each site.

## 2.9 Specific Heat of Biomass Components

Specific heat of biomass was calculated for each vegetation component at each site after Michiles and Gielow (2008) as:

$$C_B = \frac{C_{CEL} + q_{VEG}C_W}{1 + q_{VEG}} \quad [22]$$

Where  $C_B$  is a function of the specific heat of cellulose ( $C_{CEL}$ , J kg<sup>-1</sup> °C<sup>-1</sup>), the moisture content ( $q_{VEG}$ , kg kg<sup>-1</sup>), and the specific heat of water ( $C_W$ , approximated as 4186 J kg<sup>-1</sup> °C<sup>-1</sup>) for each species or vegetation component.  $R_{WD}$  of stems and leaves for species considered in this study (Aplet and Vitousek, 1994) was used to calculate  $q_{VEG}$  as:

$$q_{VEG} = \frac{mass\ H_2O}{mass\ dry} \quad [23]$$

For litter and epiphytes,  $R_{WD}$  determined from laboratory analysis directly following field collection was used. The  $R_{WD}$  of CWD was not measured, and thus was arbitrarily chosen to be 3, which was lower than epiphytes (3.67), but higher than litter (2.48).  $C_B$  was calculated separately for native tree stems, native tree leaves, *Cibotium* spp. stems, *P. cattleianum* stems, CWD, leaves, litter, and epiphytes. For native stems and leaves that were grouped together into a single compartment (*M. polymorpha*, *I. anomala*, and *C. trigynum*), the mass weighted average of  $C_B$  for all species was used. A sensitivity test by Oliphant et al. (2004) demonstrated changing  $C_B$  has a small effect on  $Q_B$ .

## 2.10 Energy Storage in Biomass, Air, and Soil

For each vegetation component at each level in the canopy for each 30 minute period,  $Q_B$  was quantified following Equation 3. Total  $Q_B$  is calculated as the sum of all biomass components for each 30 minute period. While  $Q_A$  was calculated from 4 vertical temperature profile measurements and one relative humidity sensor at each site following Giambelluca et al. (2009) as:

$$Q_A = z_A \frac{dT_{AIR}}{dt} (C_P \rho_{DRY} + C_W q) + Z_A \frac{dq}{dt} \lambda \quad [24]$$

where  $z_A$  is the depth of the air layer (25 m and 18.3 m at Nahuku and 'Ōla'a, respectively),  $dT_{AIR}$  ( $^{\circ}C$ ) is the change in mean air layer temperature over the time interval  $dt$ ,  $C_P$  (approximated as  $1004 \text{ J kg}^{-1} \text{ }^{\circ}C^{-1}$ ) is the specific heat of dry air at constant pressure,  $\rho_{DRY}$  ( $\text{kg m}^{-3}$ ) is the density of dry air,  $q$  ( $\text{kg m}^{-3}$ ) is water vapor density,  $dq$  ( $\text{kg m}^{-3}$ ) is the change in water vapor over the time interval  $dt$ , and  $\lambda$  ( $\text{J kg}^{-1}$ ) is the latent heat of vaporization, estimated as a function of temperature. While acknowledging that humidity profiles do exist in these dense forests affecting the latent heat storage flux, below canopy relative humidity data are not available at these sites, so  $q$  is assumed constant with height.

Both  $G$  and  $Q_S$  were calculated as:

$$G = \frac{SHF_1 + SHF_2 + SHF_3 + SHF_4}{4} \quad [25]$$

and

$$Q_S = \frac{dT_{SOIL}}{dt} \times z_{SOIL} (\rho_{BD} C_S + \rho_W W_V C_W) \quad [26]$$

where  $SHF_{1-4}$  ( $W m^{-2}$ ) are outputs from soil heat flux plates,  $dT_{SOIL}$  is the two sensor average temperature change over the time interval  $dt$ ,  $z_{SOIL}$  is the depth above the heat flux plates but below the litter layer (0.08 m),  $\rho_{BD}$  ( $kg m^{-3}$ ) is the soil bulk density,  $C_S$  is the specific heat for mineral soil ( $J kg^{-1} ^\circ C^{-1}$ ),  $\rho_W$  is the density of water (approximated as  $1000 kg m^{-3}$ ), and  $W_V$  is the volumetric soil moisture content ( $m^3 m^{-3}$ ). The bulk density of the top 8 cm of soil surface was estimated to be  $255 \pm 46 kg m^{-3}$  and  $214 \pm 67 kg m^{-3}$  based on 5 and 7 surface soil samples at Nahuku and 'Öla'a, respectively. Two sampling rings (approximately 5 cm diameter and 5 cm height) were inserted into a stainless steel corer and attached to a slide hammer. To make sure the soil samples were not compressed and that soil deeper than 8 cm was not included in the samples, the slide hammer was used to drive the corer vertically into the surface of the soil below the litter later until the soil filled the bottom sampling ring and did not penetrate the top sampling ring more than 3 cm. The sampling rings were then removed from the corer and soil extending from either side of the bottom sampling ring was carefully cut off with a knife. Samples were oven dried at  $105 ^\circ C$  for 24 hours, and weighed to determine  $\rho_{BD}$  as the dry weight divided by the sample volume of  $92.92 cm^3$ , which was determined from caliper measurements of sampling rings.

At Nahuku, slowly decomposing leaf litter and fallen branches built up over time where the sensors were installed, effectively increasing the depth of the soil above the heat flux plates. This effect was revealed at Nahuku (although not at 'Öla'a) by observing a steady decrease in the annual mean diurnal cycle over 7 successive years of data collection (2004–2011). To apply a correction factor at Nahuku,  $G$  and  $Q_S$  were summed for each time period, and the standard deviation of annual values of  $G + Q_S$  was divided by the standard deviation of annual values of the sum of  $G$  and  $Q_S$  for the second year of installation (2006). In the 6<sup>th</sup> year (2010), the standard deviation of  $G$  was 64 % of the second year, so the correction applied for this year was 1.56. Each 30 minute value in the time series was divided by this ratio on an annual basis.

Because these two terms were lumped to apply the correction factor from here on G and Q<sub>s</sub> (heat flux into and out of the soil surface, below the litter layer) will be grouped together into a single term (G) when considering the effects on energy closure.

### 2.11 Effects of Environmental Parameters on Energy Closure

Relative energy closure and EI<sub>ABS</sub> are evaluated considering inclusion of various heat storage terms, time of day, u\*, and ξ. Evaluation of the effect of u\* was analyzed separately for daytime and night-time periods based on solar radiation and, because night-time periods have lower energy closure for a given u\* value due to stable atmospheric conditions. Atmospheric stability was quantified according to a buoyancy parameter as:

$$\xi = \frac{z-z_0}{L} \quad [27]$$

where z (m) is the measurement height, z<sub>0</sub> (m) is the zero plane displacement height (estimated as seven-tenths of the canopy height (Bonan, 2008, p. 208), and L is the Obukhov length scale, given as:

$$L = - \frac{u^*}{k \frac{g}{\theta_V} \times \frac{H_V}{\rho C_P}} \quad [28]$$

where g is the acceleration of gravity (9.81 m s<sup>-2</sup>), k is the von Karman constant (0.41), θ<sub>V</sub> (K) is the virtual potential temperature at the surface, ρ<sub>A</sub> (kg m<sup>-3</sup>) is the air density, and H<sub>V</sub> (W m<sup>-2</sup>) is the virtual sensible heat flux. θ<sub>V</sub> is approximated as:

$$\theta_V = \theta(1 + 0.61q) \quad [29]$$

where q (kg m<sup>-3</sup>) is the water vapor concentration, and

$$H_V = H + 0.61C_P LE \quad [30]$$

Positive values of  $\xi$  represent stable conditions, while negative values represent unstable conditions, and near zero values of  $\xi$  represent neutral conditions. Median  $\xi$  and mean  $u^*$  of equal-sized bins are evaluated as a function of  $\Omega$  and  $El_{ABS}$  for two treatments: 1) available energy set equal to net radiation minus soil heat flux ( $R_{NET} - G$ ,  $W m^{-2}$ ) and 2) available energy set equal to net radiation minus the sum of heat storage in the soil, biomass, and air ( $R_{NET} - Q_{SUM}$ ,  $W m^{-2}$ ). Median  $\xi$  is used in place of the mean so as to limit the influence of extreme cases of stable or unstable conditions. While  $\xi$  and  $u^*$  are not independent, both were used to allow comparison with past research. The difference between the two treatments for each measure of energy closure over various atmospheric conditions is expected to highlight the environmental conditions when combined  $Q_B$  and  $Q_A$  are most significant regarding energy closure. To provide a measure of the fit of the regression lines to the data, the root mean square error (RMSE) and the standard error of the regression coefficient  $\Omega$  ( $S_B$ ) for each bin are determined as:

$$RMSE = \sqrt{\frac{\sum_{i=1}^n (y_i - \hat{y}_i)^2}{n}} \quad [31]$$

and

$$S_B = \frac{RMSE}{\sqrt{\sum_{i=1}^n (x_i - \bar{x})^2}} \quad [32]$$

Where  $y_i$  is the value of  $LE + H$ ,  $\hat{y}_i$  is the predicted value of  $LE + H$  for each observation  $i$ ,  $x_i$  is the measured value of  $R_{NET} - Q_{SUM}$  or  $R_{NET} - G$ , and  $\bar{x}$  is the mean value of  $R_{NET} - Q_{SUM}$  or  $R_{NET} - G$  for each bin.

## CHAPTER 3. RESULTS

### 3.1 Fresh Biomass Estimates

Fresh biomass of the dominant tree species, dead organic matter, and epiphytes estimated from surveys, laboratory analysis, and allometric equations is displayed in Table 3.1 for both sites. The total fresh biomass at each site ( $B_F$ ,  $\text{kg m}^{-2}$ ) at Nahuku ( $69.8 \text{ kg m}^{-2}$ ) was estimated to be lower than at 'Ōla'a ( $75.9 \text{ kg m}^{-2}$ ). However, a t-test revealed that biomass between the two sites were not statistically different based on variability between  $100 \text{ m}^2$  plots. On average, *M. polymorpha* represented 77.2% and 21.8% of the total biomass at Nahuku and 'Ōla'a, respectively. The dominant biomass component at 'Ōla'a is *Cibotium* spp. (30.6% of  $B_F$ ) while at Nahuku, *Cibotium* spp., the dominant species in the subcanopy represents only 4.5% of  $B_F$ . At Nahuku, considerably more fine litter has accumulated above the soil surface, while at 'Ōla'a CWD was the major component of dead organic matter. Plot variability of biomass is higher at 'Ōla'a than at Nahuku, with coefficients of variation of 21.9% and 16.8%, respectively, which is likely the cause of the more diverse and uneven forest canopy at 'Ōla'a. Acknowledging the surveys may not wholly characterize the eddy covariance footprint at 'Ōla'a, results of biomass estimates are moderately consistent among plots (Table 2.1), and based on plot variability, the major tree species and approximate relative distributions of trees in the fetch of the eddy covariance sensors appear to be well represented in these plots. Invasive *P. cattleianum* accounted for 21.7% of  $B_F$  at 'Ōla'a, although stem density was nearly an order of magnitude higher than any other species at both sites. Table 3.2 presents mean biomass for each compartment of energy storage that  $T_S$  was measured or  $T_C$  modeled, showing the vertical and radial distribution of biomass at each site.

### 3.2 Temperature Measurements and Modeling

A sample 3-day period of *M. polymorpha* (Nahuku) and *P. cattleianum* ('Ōla'a)  $T_S$  (four sensor average) and  $T_C$  temperature measurements are shown in Figure 3.1, illustrating the large variability between sunny (7/19/2007) and cloudy days (7/21/2007). Table 3.3 presents the organization of measured temperature data used to predict  $Q_B$  for the annular portion of stem

volume for the duration of the analysis, including temperature sensor locations, mean diurnal temperature range, and parameters used to estimate  $Q_B$  for each compartment. Table 3.4 presents data used to model the temperature at the weighted average depth of the center of mass of the core in each stem compartment at both sites, including the height range of stems ( $H_{T_{RANGE}}$ , m), the height of the temperature measurements ( $H_T$ , m),  $zT_C$ ,  $zT_{MC}$ ,  $TR_{MC}$ ,  $\alpha$ , lag,  $C_B$ , and for reference  $B_S$ .

### 3.3 Heat Storage flux in the Biomass, Air, and Soil

Diurnal cycles of heat storage terms are shown in Figure 3.2 for both sites. At Nahuku the average maximum and minimum daily values of  $Q_B$  occur at 11:00 and 18:30 with values of  $27.0 \pm 17.1 \text{ W m}^{-2}$  and  $-18.2 \pm 9.9 \text{ W m}^{-2}$ , respectively. At 'Ōla'a, the average diurnal maxima and minima of  $Q_B$  are  $48.3 \pm 29.2 \text{ W m}^{-2}$  at 09:30 and  $-29.3 \pm 14.9$  at 18:00, respectively. The earlier diurnal maximum at 'Ōla'a compared to Nahuku is presumably due to 'Ōla'a having a higher proportion of smaller stems, for which a greater proportion of biomass is near the outer surface. Figure 3.3 shows  $Q_B$  separated into its major components: native trees, tree ferns, foliage and epiphytes, dead organic matter, and *P. cattleianum*. While *M. polymorpha* largely dominates  $Q_B$  at Nahuku, a mixed contribution of biomass components characterizes  $Q_B$  at the 'Ōla'a stand, with tree stems and foliage contributing more in the morning and lower canopy elements like tree ferns and dead organic matter contributing more in the middle of the day. At Nahuku,  $Q_A$  has a maximum of  $14.1 \pm 13.7 \text{ W m}^{-2}$  at 08:00 and a minimum of  $-8.8 \pm 9.8 \text{ W m}^{-2}$  at 18:00, and at 'Ōla'a  $Q_A$  has a maximum of  $15.1 \pm 12.0 \text{ W m}^{-2}$  at 08:00 and a minimum of  $-5.6 \pm 5.6 \text{ W m}^{-2}$  at 18:30. Interestingly, on average  $Q_A$  is larger at 'Ōla'a than at Nahuku, although the Nahuku air layer below the instruments is 7 m thicker. While it is possible that  $Q_A$  is prone to error because humidity was assumed to be constant with height in the canopy when estimating  $Q_{LE}$ , humidity profile measurements are currently being installed at Nahuku to identify the error in  $Q_A$  caused by this assumption. As shown by Figure 3.2,  $G$  contributes a small but significant fraction of the total heat storage flux at both sites and the mean peak positive and negative fluxes are considerably delayed compared to  $Q_A$  and  $Q_B$ . At Nahuku,  $G$  reaches a maximum at 14:30 of  $5.9 \pm 3.6 \text{ W m}^{-2}$  and a minimum of  $-4.0 \pm 2.1 \text{ W m}^{-2}$  at 06:30. At 'Ōla'a,  $G$  reaches a maximum at 14:00 of  $7.2 \pm 3.2 \text{ W m}^{-2}$  and a minimum of  $-5.2 \pm 3.0 \text{ W m}^{-2}$  at 07:00. The mean diurnal cycles of

heat storage in each of three vertical biomass layers and biomass and in the soil to  $Q_B$  above the heat flux plates is plotted in Figure 3.4. In Figure 3.5 the mean diurnal cycle of mass specific  $Q_B$  ( $W m^{-2} kg^{-1}$ ) is plotted for each vertical layer (biomass and upper soil layer). The mean diurnal cycles of the ratios of  $Q_B$ ,  $Q_A$  and  $Q_{SUM}$  to  $R_{NET} - G$  are plotted in Figure 3.6, with daytime and night-time data plotted separately. During the morning, heat storage in the air and biomass decreases the amount of energy available for turbulent fluxes. After 15:00, energy is released from the air and biomass, effectively increasing available energy through the night.

### 3.4 Energy Closure and the Importance of Including Heat Storage

To illustrate the effects of including energy storage terms in energy balance closure analysis, the mean diurnal cycles of the absolute energy imbalance are shown for  $R_{NET} - LE + H$ ,  $R_{NET} - G - LE + H$ , and  $R_{NET} - Q_{SUM} - LE + H$  for both sites in Figure 3.7. At Nahuku, inclusion of heat storage terms reduced the energy imbalance during the day. However a significant energy imbalance remains with a mean daytime  $EI_{ABS}$  value of  $71.3 W m^{-2}$ , corresponding to a daytime relative energy deficit of 19.5%. Because  $G$  is a minor component of the energy balance at these sites (Figures 3.2, 3.7) and the purpose of this analysis is to determine improvement due to storage terms less often included in surface energy budget studies ( $Q_B$  and  $Q_A$ ), the effect of subtracting  $G$  from  $R_{NET}$  is not evaluated in regards to  $\Omega$ . Figure 3.8 shows the improvement in  $\Omega$  (moves closer to unity) as a result of including  $Q_B$  and  $Q_A$ . At Nahuku,  $\Omega$  for all available data (day and night) increased modestly from 0.767 to 0.805 after inclusion of  $Q_B$  and  $Q_A$ . At 'Ōla'a  $\Omega$  increased more significantly from 0.919 to 0.998 after inclusion of  $Q_B$  and  $Q_A$ , nearly double the estimated improvement at Nahuku.

### 3.5 Effects of Environmental Variability on Energy Closure

The mean diurnal cycles of  $u^*$  and  $\xi$  are plotted in Figure 3.9, demonstrating how atmospheric conditions change throughout the day as well as differences in the atmospheric turbulence and stability characteristics at the two sites. At Nahuku, mean diurnal  $u^*$  is considerably higher than at 'Ōla'a, due to higher average wind speed, a result of its more exposed location near the

summit of Kilauea Volcano. While daytime  $\xi$  is similar at the two sites, 'Ōla'a is characterized by more stable night-time conditions as well as slightly more unstable conditions when instability is at its maximum in the mid to late morning.

Figure 3.10a–d demonstrates the relationship between  $u^*$  and  $\Omega$  for daytime and night-time periods at both sites. While  $\Omega$  approaches 1 at 'Ōla'a after inclusion of  $Q_B$  and  $Q_A$ ,  $\Omega$  increases during daytime periods from 0.88 for the lowest  $u^*$  bin to 1.02 as mean  $u^*$  increases, reaching its maximum when  $u^*$  is approximately  $0.6 \text{ m s}^{-1}$  before leveling off. At Nahuku, maximum  $\Omega$  of 0.836 occurs when  $u^*$  is approximately  $0.42 \text{ m s}^{-1}$  after inclusion of  $Q_B$  and  $Q_A$  in the energy balance. In contrast, at Nahuku, where highly turbulent conditions represent 39.5% of available daytime periods,  $\Omega$  decreases slightly to 0.802 for  $u^*$  values greater than  $0.75 \text{ m s}^{-1}$ . Relative energy closure plotted as a function of  $u^*$  shows that the overall energy closure is reduced under low  $u^*$  conditions, both at night and during the day. The coefficient of determination for all night-time data is very low ( $r^2 < 0.2$ ), although for daytime periods the investigators have much higher confidence that the eddy covariance instruments are functioning properly ( $r^2 > 0.8$  for all bins). Figure 3.10e–h shows the relationship between  $u^*$  and  $E_{\text{ABS}}$  for daytime and night-time periods at both sites. At Nahuku, the absolute value of  $E_{\text{ABS}}$  was minimized during the night after inclusion of biomass and air heat storage, with the average night-time value changing from  $-25.6 \pm 40.7$  to  $-12.8 \pm 41.1 \text{ W m}^{-2}$ .  $E_{\text{ABS}}$  reaches  $-1.7 \text{ W m}^{-2}$  after including heat storage when  $u^*$  is  $0.43 \text{ m s}^{-1}$ , although the mean imbalance becomes more negative when  $u^*$  is above or below this value. Conversely, at 'Ola'a,  $E_{\text{ABS}}$  changes sign at night after inclusion of  $Q_{\text{SUM}}$ , changing from a mean nighttime value of  $-11.4 \pm 44.7 \text{ W m}^{-2}$  to  $10.1 \pm 44.2 \text{ W m}^{-2}$ . At 'Ōla'a,  $E_{\text{ABS}}$  appears to be independent of  $u^*$ , however standard deviations of  $E_{\text{ABS}}$  increase for larger values of  $u^*$ .

While  $\Omega$  is reduced for stable atmospheric conditions at both sites, the patterns of energy closure in relation to  $\xi$  are unique for each individual site (Figure 3.11a, b). At both sites  $\Omega$  reaches a maximum for the most unstable conditions. However,  $\Omega$  at 'Ōla'a is lower for a given value of  $\xi$  and  $u^*$ , with a much greater diurnal range of variability than Nahuku where nocturnal  $\Omega$  approaches nearly the same slope as during the day with  $u^*$  above  $0.35 \text{ m s}^{-1}$  (Figure 3.11a

The mean absolute energy imbalance as a function of stability, with error bars set to  $\pm$  one standard deviation (Figure 3.11c, d) reveals that the greatest reduction of  $E_{\text{ABS}}$  occurs for the most unstable conditions, although both mean absolute and relative cases, errors increase

with increasing in  $\Omega$  and  $EI_{ABS}$  resulting from inclusion of heat storage in the biomass and air occur during the most unstable conditions, and the smallest differences occur during less unstable conditions. For stable conditions however, there is no apparent trend in the effect of including heat storage terms on  $EI_{ABS}$  with varying atmospheric conditions.

The diurnal cycle of  $\Omega$  is plotted in Figure 3.12 for both treatments,  $R_{NET} - G$  and  $R_{NET} - Q_{SUM}$ . At both sites, including heat storage had a positive influence on  $\Omega$  in the morning, and a less pronounced negative influence in the evening. Including  $Q_B$  and  $Q_A$  for the period 08:00 to 10:00 AM, increases  $\Omega$  from 0.753 to 0.848 at Nahuku and from 0.854 to 1.031 at 'Ōla'a. Conversely, in the afternoon from 15:00 to 17:00,  $\Omega$  decreases from 0.815 to 0.793 at Nahuku and from 0.974 to 0.914 at 'Ōla'a as a result of including heat storage.

## CHAPTER 4. DISCUSSION

### 4.1 Evaluation of Fresh Biomass and Energy Storage Estimates

The two forest sites discussed in this Thesis were found to have relatively high  $B_F$  estimates for low to medium statured forests. Biomass components that are often neglected (i.e. litter, CWD, understory, and epiphytes) make up a significant proportion of  $B_F$  at these sites (Table 3.2). Compared to other estimates of  $B_F$  in forests (Table 4.1), the biomass at Nahuku and 'Ōla'a are high for their relatively low canopy height, 12–20 m and 6–16 m, respectively. Fresh biomass of a 40 m temperate eucalyptus stand in Australia (Haverd et al., 2007) and a 14–25 m tropical forest in the Amazon (Michiles and Gielow, 2008) with 66–73 kg m<sup>-2</sup> and 72.4 kg m<sup>-2</sup>, respectively, was similar to that of Nahuku and 'Ōla'a. However, despite the lower canopy height at the two montane tropical rainforest sites discussed in this thesis, *M. polymorpha* and *P. cattleianum* have relatively high wood density (both approximately 0.69 kg m<sup>-3</sup>), and Nahuku is dominated by *M. polymorpha*. At 'Ōla'a, both *M. polymorpha* and *P. cattleianum* make up a considerable portion of the biomass. Abundant subcanopy *Cibotium* spp. and accumulated CWD contribute significantly to  $B_F$  at 'Ōla'a, a very dense forest for its height. While *M. polymorpha* stems dominate  $Q_B$  at Nahuku, the substantial litter layer of approximately 10 cm depth is an important heat sink as well, absorbing heat that would otherwise penetrate the soil. Trees at Nahuku have larger mean  $D_{BH}$  which translates to a higher proportion of insulated core biomass reducing the capacity to store heat compared to a forest of similar biomass with many small stems such as 'Ōla'a. The model predicted significantly more heat absorbed by the above ground biomass at 'Ōla'a (Figure 3.2), a result of the combination of slightly higher  $B_F$  with numerous small *P. cattleianum* stems and fallen and standing *Cibotium* tree ferns. Haverd et al. (2007) predicted higher heat storage for smaller stems for a given biomass, consistent with the results of this study.

The results of the analysis of heat storage by different biomass components indicate that each of the components shown in Figure 3.3 contribute significantly for different parts of the day, and site variability influences the magnitude and timing of heat storage fluxes. Biomass elements positioned higher up in the canopy with smaller diameter stems are more exposed to direct radiation and store and release more energy for a given mass. The contribution of the lowest biomass layer to  $Q_B$  is the highest among the three layers at both sites because of higher

biomass density near the surface, and the highest layer contributes significantly despite low biomass in the uppermost layer (Figures 3.4, 3.5). For example, at 'Ōla'a, while only 18% of  $B_F$  is above 6 m (the highest layer), this layer contributes 32% of  $Q_B$ . At Nahuku, where only 10% of  $B_F$  is above 12 m (the highest layer), this layer contributes 18% of  $Q_B$ .

While dense forest canopies may limit productivity in the understory for many native plants, species that thrive in low light conditions such as *P. cattleianum* can thicken a forest compared to undisturbed native forest. However, since native species generally do not germinate in the presence of *P. cattleianum* due to dark shade and possible alleotropic activity at the soil surface, the mixed invaded forest 'Ōla'a is being slowly replaced by a monotypic stand of *P. cattleianum*.

It was qualitatively reasoned that the major sources of error in determining  $Q_B$  and  $Q_A$  may be the predictive power of biomass allometric equations, the representativeness of biomass surveys and temperature measurements, and the lack of an air humidity profile. Tropical forests with mixed structure, such as 'Ōla'a are difficult to correctly scale survey and temperature measurements to the stand level. However, the method proposed in this study confronted the problem of limited survey capability and temperature measurements with a rigorous evaluation of biomass components, and an averaging method where temperature measurements are evaluated at the weighted average center of mass of a quantified volume.

The standard deviations of  $B_F$  between 10 x 10 m plots at Nahuku (8 plots) and 'Ōla'a (6 plots) were used to run a sensitivity test of the effect on energy closure with changing  $B_F$ , one of the possible sources of error described above. Assuming the proportions of inner and outer biomass remain the same,  $Q_B$  is directly proportional to  $B_F$ . At Nahuku and 'Ōla'a, the standard deviations of  $B_F$  are 11.7 kg m<sup>-2</sup> and 16.6 kg m<sup>-2</sup>, which represent 16.8% and 21.9% of mean  $B_F$  for each site. At Nahuku, this error corresponds to a change in  $\Omega$  of  $\pm 0.007$ , and the mean night-time imbalance changes  $\pm 2.3$  W m<sup>-2</sup>. At 'Ōla'a, the error corresponds to a change in  $\Omega$  of  $\pm 0.014$ , and the mean night-time imbalance changes  $\pm 3.9$  W m<sup>-2</sup>.

#### 4.2 Energy Closure in Relation to Environmental Variability

When all components of biomass are considered in the energy balance on a sub-hourly basis the results indicate significant improvement of relative and mean absolute energy closure. The

greater improvement of  $\Omega$  at 'Ōla'a is the result of the larger diurnal range of  $Q_B$  and  $Q_A$  at 'Ōla'a (Figure 3.2). However, the RMSE and  $r^2$  did not change significantly after heat storage corrections, i.e., including heat storage does not increase the predictive power of the regression between available energy and turbulent flux. However, the theoretical foundation of including heat storage stands despite this limitation.

During unstable daytime conditions, convectively driven turbulence is sufficient for valid eddy covariance flux measurement at both sites. However at 'Ōla'a, somewhat higher frequency of lower wind speeds contribute to lower availability of data with sufficient  $u^*$  to accurately measure LE and H (Figure 3.10b). Lower nocturnal  $\Omega$  found at both sites (particularly at 'Ōla'a) is not anticipated to significantly influence results regarding direct ET measurements, as LE is expected to be low during the night when stable atmospheric conditions contribute to a reduced ability to measure fluxes. Unlike respiration which does not depend on atmospheric  $CO_2$  concentration, ET will be suppressed as water vapor concentration builds up within the canopy. However, because  $CO_2$  fluxes are often measured alongside water vapor fluxes using the same instrumentation, it is important to note that lower nocturnal energy closure may be indicative of a reduced ability to measure  $CO_2$  fluxes (Barr et al., 2006), which is of particular concern at 'Ōla'a.

The magnitude of the remaining daytime  $EI_{ABS}$  after inclusion of heat storage at Nahuku implies that although some improvement is apparent, including heat storage does not close the energy balance at this site (Figure 3.7a). It is possible that larger turbulent structures described in section 1.2 are responsible for the lack of energy closure. Conversely at 'Ōla'a, while including heat storage increased  $\Omega$  to near 1 over most environmental conditions during the day and reduced the absolute value of  $EI_{ABS}$  for all periods of the day, it also resulted in changing the sign of  $EI_{ABS}$  for both daytime and night-time periods (Figure 3.7b). The small mean energy surplus during the day and positive imbalance at night are possibly a result of overestimation of  $Q_B$  at this site, a consequence that cannot be ruled out due to the complexity of the forest described in section 2.1. The diversity and patchiness at the 'Ōla'a forest site introduces greater error when scaling up temperature and biomass from limited observations. Compared to 'Ōla'a, results at Nahuku are expected to be more reliable due to the uniformity of the *M. polymorpha*-dominated stand of similar age and structure, and availability of site- and species-specific allometry. Because it is possible that temperature measurements were not representative of the complex distribution of biomass at the 'Ōla'a site, or further that the limited surveys do not

accurately represent the average biomass distribution of the entire footprint of the turbulent flux measurements, estimates of energy storage at this site are subject to larger error.

As in this study, Lindroth et al. (2010) also reported  $E_{ABS}$  increasing from negative closer to zero after inclusion of  $Q_{SUM}$  (Figure 3.10g, h). The difference between mean night-time course of  $R_{NET} - G$  and 0 may be a good indicator of the magnitude of heat storage terms. However, since turbulent fluxes are not well represented at night, it is not conclusive whether the magnitude of night-time  $E_{ABS}$  before inclusion of  $Q_A$  and  $Q_B$  is a proper measure of those heat storage terms.

Results from three boreal forest stands (Barr et al., 2006) found that, at all sites, daytime  $\Omega$  continued to increase with increasing  $u^*$  without reaching a maximum. In the present study,  $\Omega$  levels off above a certain  $u^*$  value, indicating that turbulence is sufficient for reliable eddy covariance measurements under most daytime conditions, especially at Nahuku (Figure 3.10c, d). In the daytime at Nahuku, less than 10% of available data was affected by low  $u^*$  below  $0.2 \text{ m s}^{-1}$ , although slightly lower energy closure also occurs for higher  $u^*$  values above  $0.7 \text{ m s}^{-1}$ . At 'Öla'a  $\Omega$  was reduced with  $u^*$  below  $0.5 \text{ m s}^{-1}$ , which represents approximately half of the available data at this site. While  $\Omega$  improves with increasing  $u^*$  until a threshold is met at both sites,  $E_{ABS}$  is much larger for high  $u^*$  values that generally occur during the day. However at 'Öla'a,  $E_{ABS}$  remains comparatively steady with increasing  $u^*$ .

The variation in the effect of including heat storage on  $\Omega$  according to the time of day at these sites is arguably one of the more significant findings of this analysis (Figure 3.12). Heat storage corrections provided a positive influence on  $\Omega$  in the morning and a less pronounced negative influence in the evening, which is interpreted to be the result of the maximum rate of increase of stored heat in the biomass and air occurring early in the day, causing this to be the time of day when accounting for heat storage is most important. When  $Q_B$  and  $Q_A$  become negative in the afternoon, available energy is consequently reduced and, therefore,  $\Omega$  decreases as a result of including heat storage.

#### 4.3 Gap-filling of Sensible and Latent Heat Fluxes

Results of these analyses illustrate the need for concurrently measuring biomass and air temperature and humidity profiles when conducting field-based eddy covariance and energy

balance studies. Because of the large proportion of missing data due to wet sensors at the study sites, gap-filling of H and LE must be carefully considered in order to limit bias. In this study, the hypothesis was advanced that regression  $R_{NET} - Q_{SUM}$  the independent variable would provide more reliable estimates of LE and H, for gap filling purposes for example, than would a regression based on  $R_{NET} - G$ . However, because it did not significantly change the predictive power of the regression, including  $Q_B$  and  $Q_A$  cannot be expected to significantly improve gap filling based on the regression method. However, it is important to note that the predictive power of the regression between available energy and H did improve somewhat after inclusion of heat storage, although the predictive power of the regression between available energy and LE was slightly lower.

#### 4.4 Evapotranspiration Adjustments Based on Energy Closure

At Nahuku, while energy closure improvement due to inclusion of heat storage is and does not come close to closing the energy balance, the effects on annual ET estimates are more significant. The ratio  $1/\Omega$  is often used as a factor to adjust LE, and hence ET, usually upward to achieve energy closure. This correction assumes that radiation measurements and energy storage estimates are more accurate than turbulent flux measurements. The missing energy is attributed to underestimation of turbulent fluxes due to stable atmospheric conditions, low wind speeds, and higher and lower turbulent motions that eddy flux instruments can capture. Under this assumption, it is important to note that including heat storage will reduce the magnitude of the energy closure adjustment. However, because the discrepancy between the turbulent flux and energy balance measurements, and energy closure characteristics differ between sites, it might be better to report flux estimates at a particular site as a possible range of values, somewhere between the measurements and the energy-closure-adjusted values.

## CHAPTER 5: CONCLUSIONS

The significant findings of this study regarding the contribution of heat storage in biomass and air layers to the energy balance are as follows:

- Estimates of  $B_F$  at the two study sites are high for their respective canopy heights, and are at the higher range of biomass estimates of land covers where heat storage has been previously evaluated.
- The amplitude of the mean diurnal course of biomass heat storage was estimated to be 30% larger at 'Ōla'a than at Nahuku despite only 9% higher estimated biomass, which is the result of a much higher proportion of small diameter stems at 'Ōla'a.
- With the exception of highly stable night-time conditions with low  $u^*$  at the 'Ōla'a site, inclusion of  $Q_B$  and  $Q_A$  in the energy balance increased  $\Omega$ , moving it closer to 1 and reduced the mean energy imbalance at both sites over the range of environmental conditions monitored.
- After including biomass, air, and soil heat storage in the calculation of energy balance, the energy closure was approximately balanced at 'Ōla'a. However a relative energy closure deficit of 19.5% remained at Nahuku, an indication that while including commonly neglected heat storage sinks may be the main reason for lack of energy closure at some sites, other sites are subjected to flux losses that must be attributed to other factors, such as lower or higher frequency turbulent structures that the eddy covariance instruments fail to measure.
- Environmental factors such as  $u^*$ ,  $\xi$ , and time of day all have unique relationships with  $\Omega$ , and these relationships change after inclusion of  $Q_B$  and  $Q_A$ .
- Inclusion of  $Q_B$  and  $Q_A$  in the energy balance was found to increase  $\Omega$  the most under the following environmental conditions: in the early morning, the most unstable atmospheric conditions, for lower  $u^*$  during the daytime and for higher  $u^*$  at night.
- At both sites after inclusion of all heat storage terms,  $\Omega$  reaches a maximum for the most unstable atmospheric conditions and in the early morning, and the lowest  $\Omega$  occurs during conditions of low  $u^*$ .

The results of this investigation suggest that site variability influences the turbulent flows above the canopy, affecting the instruments ability to measure fluxes. While the mechanism that

drives the remaining lack of energy closure after inclusion of heat storage at Nahuku is unclear, it is likely that ET should be adjusted upward to account for this loss. However, it is unclear if the assumption that missing turbulent fluxes are proportionally distributed between LE and H. The results of this study would be complemented by further analysis of specific reasons for the remaining energy closure deficit during the day at this site.

It is interesting to note the differences between sites in the ability of eddy covariance measurements to accurately determine gas and energy exchange above a given land cover. While energy closure was better in the daytime at 'Ōla'a, highly stable night-time conditions with lower  $u^*$  contributed to inferior night-time energy closure. In contrast to Nahuku, its more protected location may have contributed to near-ideal flux measurement during the day, but inhibited the ability of instruments to capture the fluxes at night. The results of this analysis will contribute to more accurate estimates of ET at these Hawaiian forest sites, and will add to the limited body of literature regarding canopy heat storage in relation to energy closure.

## REFERENCES

- Alavi, N., Warland, J.S., Berg, A.A., 2006. Filling gaps in evapotranspiration measurements for water budget studies: Evaluation of a Kalman filtering approach. *Agricultural and Forest Meteorology* 141: 57–66.
- Aplet, G.H., Vitousek, P.M., 1994. An age-altitude matrix analysis of Hawaiian rain-forest succession. *Journal of Ecology* 82: 137–147.
- Arcand, N., Kagawa, A., Sack, L., Giambelluca T.W., 2008. Scaling of frond form in Hawaiian tree fern *Cibotium glaucum*: Compliance with global trends and application for field estimation. *Biotropica* 40: 686–691.
- Asner, G.P., Hughes, R.F., Vitousek, P.M., Knapp, D.E., Keddedy-Bowdoin, T., Boardman, J., Martin, R. E., Eastwood, M., Green R.O., 2008. Invasive plants transform the three-dimensional structure of rainforests. *Proceedings of the National Academy of Sciences* 105: 4519–4523.
- Asner, G.P., Hughes, R.F., Varga, T.A., Knapp, D.E., Kennedy-Bowdoin, T., 2009. Environmental and biotic controls over aboveground biomass throughout a rainforest. *Ecosystems* 12: 261–278.
- Asner, G.P., Hughes, R.F., Mascaro, J., Uowolo, A.L., Knapp, D.E., Jacobson, J., Kennedy-Bowdoin, T. Clark, J.K., 2011. High-resolution carbon mapping on the million-hectare Island of Hawaii. *Frontiers in Ecology and the Environment* 9: 434-439. doi:10.1890/100179.
- Aubinet M., 2008. Eddy covariance CO<sub>2</sub> flux measurements in nocturnal conditions: an analysis of the problem. *Ecological Applications* 18: 1368–1378.
- Baldocchi, D.D., Falge, E., Gu, L., Olson, R., Hollinger, D., Running, S., Anthoni, P., Bernhofer, C., Davis, K., Evans, R., Fuentes, J., Goldstein, A., Katul, G., Law, B., Lee, X., Malhi, Y., Meyers, T., Munger, W., Oechel, W., Paw, K. T., Pilegaard, K., Schmid, H. P., Valentini, R., Verma, S., Vesala, T., Wilson, K., Wofsy, S., 2001. FLUXNET: A new tool to study the temporal and spatial variability of ecosystem-scale carbon dioxide, water vapor, and energy flux densities, *Bulletin of the American Meteorology Society* 82: 2415–2434.
- Barr, A.G., Morgenstern, K., Black T.A., McCaughey, J.H., Nestic, Z., 2006. Surface energy balance closure by the eddy-covariance method above three boreal forest stands and implications for the measurement of the CO<sub>2</sub> flux. *Agricultural and Forest Meteorology* 140: 322–337.
- Barr, A.G., van der Kamp, G., Black T.A., McCaughey, J.H., Nestic, Z., 2012. Energy balance closure at the BERMS flux towers in relation to the water balance of the White Gull Creek watershed 1999–2009. *Agricultural and Forest Meteorology* 153: 3–13.

- Billesbach, D.P., 2011. Estimating uncertainties in individual eddy covariance flux measurements: A comparison of methods and a proposed new method. *Agricultural and Forest Meteorology* 151: 394–405.
- Bonan, G., 2008. *Ecological Climatology; Concepts and Applications*. Cambridge University Press, New York.
- Chave, J., Andalo, C., Brown, S., Cairns, M.A., Chambers, J.Q., Eamus, D., Fölster, H., Fromard, F., Higuchi, N., Kira, T., Lescure, J.-P., Nelson, B.W., Ogawa, H., Puig, H., Rie´ra, B., Yamakura, T., 2005. Tree allometry and improved estimation of carbon stocks and balance in tropical forests. *Oecologia* 145: 87–99.
- Finnigan, J.J., Clement, R., Malhi, Y., Leuning, R., Cleugh, H. A., 2003. A re-evaluation of long-term flux measurement techniques. Part I: averaging and coordinate rotation. *Boundary-Layer Meteorology* 107: 1–48.
- Fisher, J.B., Malhi, Y., Bonal, D., Humberto, R.D.R., de Araujo, A.C. Gamo, M, Goulden, M.L., Hirano, T., Huete, A.R., Kondo, H., Kumagai, T., Loescher, H.W., Miller, S., Nobre, A.D., Nouvellon, Y., Oberbauer, S.F., Panuthai, S., Roupsard, O. , Saleska, S., Tanaka, K., Nobuaki, T., Tu, K.P., von Rando, C., 2009. The land–atmosphere water flux in the tropics. *Global Change Biology* 15: 2694–2714. doi: 10.1111/j.1365-2486.2008.01813.x
- Foken, T., 2008. The energy balance closure problem—an overview. *Ecological Applications* 18: 1351–1367.
- Gerrish G., 1988. The changing carbon balance in aging *Metrosideros polymorpha* trees. Ph.D. Dissertation. University of Hawai‘i at Mānoa, Department of Botany, Honolulu, Hawai‘i. 262 pp.
- Giambelluca, T.W., Asner, G.P., Martin, R.E., Nullet, M., Huang, M., DeLay, J.K., Mudd, R.G., Takahashi, M., 2007. Impacts of alien tree invasion on evapotranspiration in tropical montane cloud forest in Hawai‘i. *Eos Trans. AGU*, 88(52), Fall Meeting Supplement, Abstract H211-02.
- Giambelluca, T.W., Martin, R.E., Asner, G.P., Huang, M., Mudd, R.G., Nullet, M.A., DeLay, J.K., Foote, D., 2009. Evapotranspiration and energy balance of native wet montane cloud forest in Hawai‘i. *Agricultural and Forest Meteorology* 149: 230–243. doi: 10.1016/j.agrformet.2008.08.004.
- Haverd, V., Cuntz, M., Leuning, R., Keith, H., 2007. Air and biomass heat storage fluxes in a forest canopy: Calculation within a soil vegetation atmosphere transfer model. *Agricultural and Forest Meteorology* 147: 125–139.
- Hendricks Franssen, H.J., Stöckli, R., Lehner, I., Rotenberg, E., Seneviratne, S.I., 2010. Energy balance closure of eddy covariance data: A multisite analysis for European FLUXNET

- stations, *Agricultural and Forest Meteorology* 150: 1553–1567. doi: 10.1016/j.agrformet.2010.08.005.
- Heusinkveld, B.G., Jacobs, A.F.G., Holtslag, A.A.M., Berkowicz, S.M., 2004. Surface energy balance closure in an arid region: role of soil heat flux. *Agricultural and Forest Meteorology* 122: 21–37.
- Jacobs, A.F.G., Heusinkveld, B.G., Holtslag, A.A.M., 2008: Towards closing the surface energy of a mid-latitude grassland. *Boundary-Layer Meteorology* 126, 125–136.
- Jung, M., Reichstein, M., Margolis, H.A., Cescatti, A., Richardson, A.D., Arain, M.A., Arneth, A., Bernhofer, C., Bonal, D., Chen, J., Gianelle, D., Gobron, N., Kiely, G., Kutsch, W., Lasslop, G., Law, B.E., Lindroth, A., Merbold, L., Montagnani, L., Moors, E.J., Papale, D., Sottocornola, M., Vaccari, F., Williams, C., 2011. Global patterns of land - atmosphere fluxes of carbon dioxide, latent heat, and sensible heat derived from eddy covariance, satellite, and meteorological observations. *Journal of Geophysical Research* 116: doi: 10.1029/2010JG001566.
- Kanda, M., A. Inagaki, M. O. Letzel, S. Raacsh, Watanabe, T., 2004. LES study of the energy imbalance problem with eddy covariance fluxes. *Boundary-Layer Meteorology* 110: 381–404.
- Kobayashi, H., Baldocchi, D.D., Ryu, Y., Chen, Q., Ma, S., Osuna, J.L., Ustin, S.L., 2012. Modeling energy and carbon fluxes in a heterogeneous oak woodland: A three-dimensional approach. *Agricultural and Forest Meteorology* 152: 83–100.
- Kume, T., Tanaka, N., Kuraji, K., Komatsu, H., Yoshifuji, N., Saitoh, T.M., Suzuki, M., Kumagai, T., 2011. Ten-year evapotranspiration estimates in a Bornean tropical rainforest. *Agricultural and Forest Meteorology* 151: 1183–1192.
- Lamaud, E., Ogee, J., Brunet, Y., Berbigier, P., 2001. Validation of eddy flux measurements above the understorey of a pine forest. *Agricultural and Forest Meteorology* 106: 187–203.
- Lee, X., Massman, W., Law, B. (Eds.), 2004. *Handbook of Micrometeorology: A Guide for Surface Flux Measurement and Analysis*. Kluwer Academic Publishers.
- Leuning, R., Zegelin, S.J., Jones, K., Keith, H., Hughes, D., 2008. Measurement of horizontal and vertical advection of CO<sub>2</sub> within a forest canopy. *Agricultural and Forest Meteorology* 148: 1777–1797.
- Lindroth, A., Mölder, M., Lagergren, F., 2010. Heat storage in forest biomass improves energy balance closure. *Biogeosciences* 7: 301–313.
- Litton, C.M., Kauffman, J.B., 2008. Allometric models for predicting aboveground biomass in two widespread woody plants in Hawaii. *Biotropica* 40: 313–320.

- Mahrt, L., 1998. Flux sampling errors for aircraft and towers. *Journal of Atmospheric and Oceanic Technology* 15: 416–429.
- Malhi, Y., Pegoraro, E., Nobre, A.D., Pereira, M.G.P., Grace, J., Culf, A.D., Clement, R., 2002. Energy and water dynamics of a central Amazonian rain forest. *Journal of Geophysical Research* 107: 8061. doi:10.1029/2001JD000623.
- Mascaro, J., Litton, C.M., Hughes, R.F., Uowolo, A., Schnitzer, S.A., 2011. Minimizing bias in tree biomass allometry: model selection and log-transformation of data. *Biotropica* 43: 649–653. doi: 10.1111/j.1744-7429.2011.00798.
- Massman, W.J., Lee, X., 2002. Eddy covariance flux corrections and uncertainties in long-term studies of carbon and energy exchanges. *Agricultural and Forest Meteorology* 113: 121–144.
- McCaughey J.H., 1985. Energy balance storage terms in a mature mixed forest at Petawawa, Ontario – A case study. *Boundary-Layer Meteorology* 31: 89–101.
- McCaughey, J.H., Saxton, W.L., 1988. Energy balance storage terms in a mixed forest. *Agricultural and Forest Meteorology* 44: 1–18.
- Meesters, A.G., Vugts, H.F., 1996. Calculation of heat storage in stems. *Agricultural and Forest Meteorology* 78: 181–202.
- Meyers, T. P., Hollinger, S. E., 2004. An assessment of storage terms in the surface energy balance of maize and soybean. *Agricultural and Forest Meteorology* 125: 105–115.
- Michiles, A., Gielow, R., 2008. Above-ground thermal energy storage rates, trunk heat fluxes and surface energy balance in a central Amazonian rainforest. *Agricultural and Forest Meteorology* 148: 917–930. doi:10.1016/j.agrformet.2008.01.001.
- Moderow, U., Feigenwinter, C., Bernhofer, C., 2007. Estimating the components of the sensible heat budget of a tall forest canopy in complex terrain. *Boundary-Layer Meteorology* 123: 99–123.
- Moderow, U., Aubinet, M., Feigenwinter, C., Kolle, O., Lindroth, A., Mölder, M., Montaganai, L., Rebman, C., Bernhofer, C., 2009. Available energy and energy balance closure at four coniferous forest sites across Europe, *Theoretical Applied Climatology* 98: 397–412. Doi:10.1007/s00704-009-0175-0.
- Moore, C.J., Fisch, G., 1986. Estimating heat storage in Amazonian tropical forest. *Agricultural and Forest Meteorology* 38: 147–168.
- Mudd, R.G., 2004. Significance of the epiphyte layer to stem water storage in native and invaded tropical montane cloud forests in Hawai'i. Senior Thesis. Global Environmental Science, University of Hawai'i at Mānoa.

- Mudd, R.G., Giambelluca, T.W., 2006. Epiphyte water retention and evaporation in native and invaded tropical montane cloud forests in Hawai'i. *Eos Trans. AGU*, 87(52), Fall Meeting Supplement, Abstract B23C-1094.
- Mueller-Dombois, D., Jacobi, J. D., Cooray, R. G., Balakrishnan, N., 1977. Ohia Rain Forest Study: Ecological Investigations of the Ohia Dieback Problem in Hawaii. CPSU Tech. Rep. 20. Honolulu: University of Hawai'i at Manoa; 117 p. + 3 maps.
- Nagler, P.L., Scott, R.L., Westenburg, C., Cleverly, J.R., Glenn, E.P., Huete, A.R., 2005. Evapotranspiration on western U.S. rivers estimated using the Enhanced Vegetation Index from MODIS and data from eddy covariance and Bowen ratio flux. *Remote Sensing of Environment* 97: 337–351.
- Oliphant, A.J., Grimmond, S.B., Zutter, H.N., Schmid, H.P., Su, H.B., Scott, S.L., Offerle, B., Randolph, J.C., Ehman, J., 2004. Heat storage and energy balance fluxes for a temperate deciduous forest. *Agricultural and Forest Meteorology* 126: 185–201.
- Oncley, S. P., Foken, T., Vogt, R. Kohsiek, W., DeBruin, H., Bernhofer, C., Christen, A., Gorsel, E., Grantz, D., Feigenwinter, C., Lehner, I., Lieberthal, C., Liu, H., Mauder, M., Pitacco, A., Ribeiro, L., Weidinger, T., 2007. The energy balance experiment EBEX-2000, Part I: overview and energy balance. *Boundary-Layer Meteorology* 123: 1–28. doi: 10.1007/s10546-007-9161-1.
- Raich, J.W., Russell, A.E., Vitousek, P.M., 1997. Primary productivity and ecosystem development along an elevational gradient on Mauna Loa, Hawaii. *Ecology* 78: 707–721.
- Reichstein, M., Papale, D., Valentini, R., Aubinet, M., Bernhofer, C., Knohl, A., Laurila, T., Lindroth, A., Moors, E., Pilegaard, K., Seufert, G., 2007. Determinants of terrestrial ecosystem carbon balance inferred from European eddy covariance flux sites. *Geophysical Research Letters* 34: L01402.262. doi:10.1029/2006GL027880.
- Sakai, R., Fitzjarrald, D., Moore, K.E., 2001. Importance of low-frequency contributions to eddy fluxes observed over rough surfaces. *Journal of Applied Meteorology* 40: 2178–2192.
- Scott, R.L., 2010. Using watershed water balance to evaluate the accuracy of eddy covariance evaporation measurements for three semiarid ecosystems. *Agricultural and Forest Meteorology* 150: 219–225.
- Silberstein, R., Held, A., Hatton, T., Viney, N., Sivapalan, M., 2001. Energy balance of a natural jarrah (*Eucalyptus marginata*) forest in Western Australia: measurements during the spring and summer. *Agricultural and Forest Meteorology* 109: 79–104.
- Silberstein, R., Sivapalan, M., Viney, N., Held, A., Hatton, T.J., 2003. Modeling energy balance of a natural jarrah (*Eucalyptus marginata*) forest. *Agricultural and Forest Meteorology* 115: 201–230.

- Smith, C. W. 1985. Impact of Alien Plants on Hawaii's Native Biota. pp. 180–250. in C. P. Stone and J. M. Scott (eds.). *Hawaii's Terrestrial Ecosystems: Preservation and Management*. University of Hawaii Cooperative National Park Resources Studies Unit, University of Hawaii Press. 584 pp.
- Sulkava, M., Luyssaert, S., Zaehle, S., Papale, D., 2011. Assessing and improving the representativeness of monitoring networks: The European flux tower network example. *Journal of Geophysical Research* 116: doi:10.1029/2010JG001562
- Takahashi, M., Giambelluca, T.W., Mudd, R.G., DeLay, J.K., Nullet, M.A., Asner, G.P., 2011. Rainfall partitioning and cloud water interception in native forest and invaded forest in Hawai'i Volcanoes National Park. *Hydrological Processes* 225: 448–464.
- Thom, A.S., 1975. Momentum, heat and mass exchange of plant communities. In: Monteith, J.L. (Ed.), *Vegetation and the Atmosphere*. Academic Press, London: pp. 57–109.
- Thomas, C.K., 2011. Variability of sub-canopy flow, temperature, and horizontal advection in moderately complex terrain. *Boundary-Layer Meteorology* 139: 61–81. doi: 10.1007/s10546-010-9578-9.
- Twine, T.E., Kustas, W.P., Norman, J.M., Cook, D.R., Houser, P.R., Meyers, T.P., Prueger, J.H., Starks, P.J., Wesely, M.L., 2000. Correcting eddy-covariance flux underestimates over a grassland. *Agricultural and Forest Meteorology* 103: 279–300.
- Vickers, D., Irvine, J., Martin, J.G., Law, B.E., 2012. Nocturnal subcanopy flow regimes and missing carbon dioxide. *Agricultural and Forest Meteorology* 152: 101–108.
- Vitousek, P.M., 1990. Biological invasions and ecosystem processes: towards an integration of population biology and ecosystem studies. *Oikos* 57: 7–13.
- Von Randow, C., Kruijt, B., Holtslag, A.A.M., De Oliveira, A.B.L., 2008. Exploring eddy-covariance and large-aperture scintillometer measurements in an Amazonian rain forest. *Agricultural and Forest Meteorology* 148: 680–690.
- Wang, R.Y., Zhang, Q., 2011. An assessment of storage terms in the surface energy balance of a subalpine meadow in Northwest China. *Advances in Atmospheric Sciences* 28: 691–698. doi: 10.1007/s00376-010-9152-x.
- Wilson, K.B., Baldocchi, D.D., 2000. Seasonal and interannual variability of energy fluxes over a broadleaved temperate deciduous forest in North America. *Agricultural and Forest Meteorology* 100: 1–18.
- Wilson, K.B., Goldstein, A., Falge, E., Aubinet, M., Baldocchi, D.D., Berbigier, P., Bernhofer, C., Ceulemans, R., Dolman, H., Field, C., Grelle, A., Ibrom, A., Law, B. E., Kowalski, A., Meyers,

- T.P., Moncrieff, J., Monson, R., Oechel, W., Tenhunen, J., Valentini, R., Verma, S., 2002. Energy balance closure at FLUXNET sites. *Agricultural and Forest Meteorology* 113: 223–243.
- Wolfe, E.W., Morris, J. 1996. Geologic map of the island of Hawaii. U. S. Geological Survey Series IMAP, Report # 2524-A.
- Yu, X., Chen, L., Niu, J., Zhao, Y., 2004. Hydrological effects of CWD in sub-alpine dark coniferous ecosystem of upper reaches of Yangtze River. *Science of Soil and Water Conservation* 2: 117–122.
- Zhu, X-G., Long, S.P., Ort, D.R., 2008. What is the maximum efficiency with which photosynthesis can convert solar energy into biomass? *Current Opinion in Biotechnology* 19: 153-159.

## TABLES

Table 2.1. Characteristics of canopy and subcanopy species in survey plots from two sites on the Big Island of Hawai'i.

Species	Stem density	Mean $D_{BH}$	$D_{BH}$ range	BA	Mean height
a) Native Site - Nahuku	$n\ ha^{-1}$	cm	cm	$cm^2\ m^{-2}$	m
<i>Metrosideros polymorpha</i>	1675	16.8 (8.5)	5.2 – 51.2	46.13	12.7 (2.9)
<i>Ilex anomala</i>	200	13.0 (11)	5.0 – 31.6	4.33	10.2 (4.7)
<i>Coprosma</i> sp.	50	6.9 (1.1)	6.1 – 7.7	0.19	8.3 (0.9)
<i>Cibotium</i> spp.	738	20.0 (8.6) <sup>A</sup>	5.0 – 33.6	40.56	3.8 (1.3)
<i>Sadleria</i> spp.	875	5.9 (1.1) <sup>A</sup>	5.1 – 9.0	2.51	1.0 (0.3)
b) Invaded Site - 'Ōla'a					
<i>Metrosideros polymorpha</i>	300	17.5 (9.7)	5.6 – 39.5	9.29	11.4 (3.2)
<i>Ilex anomala</i>	267	10.6 (6.3)	5.9 – 31.0	3.11	8.5 (2.0)
<i>Cheirodendron trigynum</i>	333	13.9 (4.2)	8.3 – 24.0	5.50	10.5 (1.9)
<i>Psidium cattleianum</i>	12467	4.2 (1.6)	2.0 – 11.7	20.44	5.5 (2.1)
<i>Cibotium</i> spp. <sup>A</sup>	3083	21.1 (5.2)	10.0 – 36.0	109.48	4.6 (1.6)

$D_{BH}$  is the diameter at breast height (1.3 m) and BA is the basal area of each species, calculated  $(D_{BH}/2)^2$ . Vegetation surveys encompassed 8 plots of 100 m<sup>2</sup> and 6 plots of 100 m<sup>2</sup> at Nahuku and 'Ōla'a, respectively. All stems greater than 5 cm included, individuals greater than 2 cm included for *P. cattleianum*. Standard deviation (in parentheses) represents combined plot variability for each species.<sup>A</sup> For *Cibotium* spp. and *Sadleria* spp., diameter measured at midpoint height of stem.

Table 2.2. Wood density (WD) and wet to dry ratio's ( $R_{WD}$ ) for stems and leaves.

Species	WD ( $g\ cm^{-3}$ )	Stem $R_{WD}$	Leaf $R_{WD}$
<i>Metrosideros polymorpha</i> <sup>A</sup>	0.69 <sup>A</sup>	1.87 <sup>B</sup>	2.11 <sup>B</sup>
<i>Cheirodendron trigynum</i> <sup>A</sup>	0.47 <sup>A</sup>	1.95 <sup>B</sup>	3.01 <sup>B</sup>
<i>Ilex anomala</i> <sup>A</sup>	0.48 <sup>A</sup>	2.22 <sup>B</sup>	2.88 <sup>B</sup>
<i>Coprosma</i> Spp. <sup>A</sup>	0.48 <sup>A</sup>	2.20 <sup>B</sup>	2.51 <sup>B</sup>
<i>Cibotium glaucum</i> <sup>A</sup>	0.22 <sup>A</sup>	2.72 <sup>B</sup>	3.16 <sup>B</sup>
<i>Psidium cattleianum</i> <sup>B</sup>	0.69 <sup>A</sup>	1.74 <sup>C</sup>	2.71 <sup>C</sup>

<sup>A</sup> Asner et al. (2011); <sup>B</sup> Applet and Vitousek (1994); <sup>C</sup> F. Hughes, USDA Forest Service, Hilo, unpublished data

Table 2.3. Regressions developed from harvested *Psidium cattleianum* trees to predict vertical and radial compartments of stem fresh biomass ( $B_S$ , g) from diameter at 1.3 m ( $D_{BH}$ , cm). RMSE is the root mean square error of the model and  $r^2$  is the coefficient of determination.

compartment	allometric equation	RMSE (g)	$r^2$
0 – 4 m core	$B_S = 1226 \times D_{BH} - 7070$	626	0.95
0 – 4 m skin	$B_S = 587 \times D_{BH}^{1.787}$	2107	0.98
4 – 6 m skin	$B_S = 423 \times D_{BH}^{1.488}$	687	0.97
6 – 10 skin	$B_S = 248 \times D_{BH}^{1.777}$	1622	0.87
<b>All stems</b>	<b><math>B_S = 1072 \times D_{BH}^{1.809}</math></b>	<b>2587</b>	<b>0.98</b>

Table 3.1. Fresh biomass ( $\text{kg m}^{-2}$ ) by component at Nahuku (a) and 'Ōla'a (b).

Species or Element	a) Native forest		b) Invaded forest	
	Stems	Foliage	Stems	Foliage
<i>Metrosideros polymorpha</i>	49.4 (19.2)	2.00 (0.7)	10.1 (14.7)	0.4 (0.5)
<i>Ilex anomala</i>	4.4 (4.0)	0.23 (0.18)	3.9 (4.2)	0.4 (0.4)
<i>Cheirodendron trigynum</i>	–	–	2.5 (2.7)	0.2 (0.2)
<i>Psidium cattleianum</i>	–	–	20.6 (12.9)	1.3 (0.9)
<i>Coprosma</i> sp.	0.1 (0.13)	0.01 (0.01)	–	–
<i>Cibotium</i> and <i>Sadleria</i> spp.	3.1 (1.50)	1.02 (0.61)	23.2 (3.4)	2.4 (1.4)
CWD	1.84 (*)		8.2 (8.3)	
Litter	6.8 (2.7)		2.4 (1.0)	
Epiphytes	0.94 (0.29)		0.3 (*)	
<b>Total</b>	<b>69.8 (11.7)</b>		<b>75.9 (16.6)</b>	

CWD is coarse woody debris (stems larger than 5 cm diameter). Standard deviation in parentheses represents plot, subplot, or combined plot variability. \*Only 2 plots measured, hence no standard deviation is given.

Table 3.2. Radial and vertical distribution of fresh biomass ( $B_s$ ,  $\text{kg m}^{-2}$ ) at Nahuku (a) and 'Ōla'a (b).

Nahuku, native forest							
Species	Core 0–6 m	Skin	Core 6–12 m	Skin	Core 12–20 m	Skin	$B_s$ % of total
Stem (native trees)	16.37	10.36	10.10	11.62	1.29	4.15	77.2
Stem (ferns)	1.52	1.70	–	–	–	–	4.5
CWD	0.31	1.53	–	–	–	–	2.6
Litter	6.76		–		–		9.7
Foliage (ferns)	1.02		–		–		1.5
Foliage (native trees)	0.03		1.00		1.25		3.3
Epiphytes	0.83		0.11		–		1.3
<b>Total</b>	<b>69.8 (11.7)</b>						
'Ōla'a, invaded forest							
Species	Core 0–4 m	Skin	Core 4–6 m	Skin	Core 6–17 m	Skin	$B_s$ % of total
Stem (native trees)	4.56	3.00	0.54	0.94	2.35	5.16	21.8
Stem (ferns)	11.80	11.45	–	–	–	–	30.6
Stem ( <i>P. cattleianum</i> )	0.42	10.86	0.01	4.80	–	4.51	27.1
CWD	4.76	3.42	–	–	–	–	10.8
Litter	2.42		–		–		3.2
Foliage (ferns)	1.44		1.44		–		3.8
Foliage (native trees)	<0.01		0.05		0.81		1.1
Foliage ( <i>P. cattleianum</i> )	0.01		0.25		0.59		1.1
Epiphytes	0.29		0.02		0.02		0.4
<b>Total</b>	<b>75.9 (16.6)</b>						

"core" represents the inner cylinder of larger stems, and "skin" represents the annulus. CWD is coarse woody debris (fallen dead stems larger than 5 cm diameter). Standard deviation (in parentheses) represents plot variability (10 m x 10 m plots) of combined fresh biomass.

Table 3.3. Parameters used to estimate energy storage in the annular portions of biomass (skin), including height range of stem sections ( $H_{t_{RANGE}}$ ), the height of temperature measurements ( $H_{t_T}$ ), depth of temperature measurement in the stem ( $z_{T_S}$ ), mean diurnal temperature range (TR), and parameters used to estimate biomass energy storage, including specific heat of biomass ( $C_B$ ) and fresh biomass ( $B_S$ ).

Component	Nahuku						‘Ōla‘a					
	$H_{t_{RANGE}}$ m	$H_{t_T}$ m	$z_{T_S}$ cm	TR °C	$C_B$ J kg <sup>-1</sup> °C <sup>-1</sup>	$B_S$ kg m <sup>-2</sup>	$H_{t_{RANGE}}$ m	$H_{t_T}$ m	$z_{T_S}$ cm	TR °C	$C_B$ J kg <sup>-1</sup> °C <sup>-1</sup>	$B_S$ kg m <sup>-2</sup>
<i>Mp</i> Skin <sup>A</sup>	0– 6	3.0	1	3.09	2608	13.71	0– 4	3.0 <sup>D</sup>	1.0 <sup>D</sup>	4.70 <sup>D</sup>	2637	3.00
<i>Mp</i> Skin <sup>A</sup>	6–12	9.0	1	3.63	2608	15.82	4– 6	5.0 <sup>D</sup>	1.0 <sup>D</sup>	6.10 <sup>D</sup>	2637	0.94
<i>Mp</i> Skin <sup>A</sup>	12–20	15.0	1	5.31	2608	5.87	6–17	7.0 <sup>D</sup>	1.0 <sup>D</sup>	6.97 <sup>D</sup>	2637	5.16
<i>Cib</i> _Skin	0– 3.5	0.5	1.5	2.65	3084	2.31	0– 4	0.5	1.5	2.62	3084	11.45
<i>Pc</i> Skin	–	–	–	–	–	–	0– 4	3.0	1.0	4.70	2460	10.85
<i>Pc</i> Skin	–	–	–	–	–	–	4– 6	5.0	1.0	6.10	2460	4.80
<i>Pc</i> Skin	–	–	–	–	–	–	6–17	7.0	1.0	6.97	2460	4.51
Foliage <sup>B</sup>	0– 6	3.0	0	4.63	2938	1.05	0– 4	3.0	0	5.13	3141	1.45
Foliage <sup>B</sup>	6–12	9.0	0	4.69	2938	1.00	4– 6	9.0	0	5.79	3141	1.74
Foliage <sup>B</sup>	12–20	25.0	0	4.80	2938	1.25	6–17	25.0	0	5.92	3141	1.40
CWD Skin <sup>C</sup>	0– 0.5	0.5	1.5	2.65	3185	1.53	0– 0.5	0.5	1.0	2.62	3185	3.42
Litter <sup>C</sup>	0– 0.1	0.5	1.5	2.65	3501	6.77	0– 0.1	0.5	1.5	2.62	3501	2.42
Epiphytes <sup>B</sup>	0– 6	3.0	0	4.63	3368	0.82	0– 4	3.0	0	5.13	3368	0.29
Epiphytes <sup>B</sup>	6–12	9.0	0	4.69	3368	0.12	4– 6	5.0	0	5.79	3368	0.02
Epiphytes <sup>A</sup>	–	–	–	–	–	–	6–17	7.0	0	5.92	3368	0.02

*Mp* = *Metrosideros polymorpha*, *Pc* = *Psidium cattleianum*, *Cib* = *Cibotium* spp. <sup>A</sup>Includes *Ilex anomala* and *Coprosma* spp., and *Cheirodendron trigynum*. <sup>B</sup> Leaf and epiphyte temperature assumed to be equivalent to air temperature. <sup>C</sup> CWD (fallen dead stems larger than 5 cm diameter) and litter temperature estimated from *Cibotium* spp. temperature at 1.5 cm. <sup>D</sup> native tree skin temperature estimated from *Pc* skin temperature at ‘Ōla‘a.

Table 3.4. Parameters used to model temperature and energy storage in the interior “core” volume of stems, including the height range that the temperature measurements were assumed to represent ( $H_{t_{RANGE}}$ ) height of temperature measurements ( $H_{t_T}$ ), depth of temperature measurement in the stem ( $z_{T_C}$ ), the modeled depth of temperature measurement at the center of mass of the stem core volume ( $z_{T_{MC}}$ ), the modeled mean diurnal temperature range ( $TR_{MC}$ ), the time lag predicted by temperature sensors at two depths (lag), and parameters used to estimate biomass energy storage such as specific heat of biomass ( $C_B$ ), and fresh biomass ( $B_S$ ).

Core Element	$H_{t_{RANGE}}$ m	$H_{t_T}$ m	$z_{T_C}$ cm	$z_{T_{MC}}$ cm	$TR_{MC}$ °C	$\alpha$ unitless	lag min $cm^{-1}$	$C_B$ $J\ kg^{-1}\ ^\circ C^{-1}$	$B_S$ $kg\ m^{-2}$
<b>Nahuku</b>									
<i>Mp</i> Core <sup>A</sup>	0– 6	3.0	4.75	5.44	1.66	1.84E-07	40	2608	16.67
<i>Mp</i> Core <sup>A</sup>	6–12	9.0	6.0	4.82	2.81	8.06E-07	30	2608	10.28
<i>Mp</i> Core <sup>A</sup>	12–20	15.0	4.5	4.69	5.15	5.35E-05	17	2608	1.30
<i>Cib</i> Core	0– 3.5	0.5	5.0	6.32	1.36	1.91E-07	34	3084	1.52
CWD Core	0– 0.5	0.5	5.0	4.90	1.66	1.91E-07 <sup>C</sup>	34	3185	0.31
<b>‘Ōla‘a</b>									
<i>Mp</i> Core <sup>B</sup>	0– 4	3.0	4.75	5.39	1.67	1.84E-07 <sup>D</sup>	40	2637	4.56
<i>Mp</i> Core <sup>B</sup>	4– 6	5.0	6.0	5.15	2.75	8.06E-07 <sup>D</sup>	30	2637	0.54
<i>Mp</i> Core <sup>B</sup>	6–17	7.0	4.0	4.55	5.16	5.35E-05 <sup>D</sup>	17	2637	2.35
<i>Cib</i> Core	0– 4	0.5	4.5	5.83	1.74	2.96E-07	22	3084	11.75
<i>Pc</i> Core	0– 4	3.0	4.0	3.21	4.65	1.67E-04	15	2460	0.42
<i>Pc</i> Core	–	5.0	3.0	No Core	–	–	–	–	0.00
<i>Pc</i> Core	–	7.0	2.0	No Core	–	–	–	–	0.00
CWD Core	0– 0.5	0.5	4.5	6.58	1.60	2.96E-07 <sup>C</sup>	22	3185	4.76

*Mp* = *Metrosideros polymorpha*, *Pc* = *Psidium cattleianum*, *Cib* = *Cibotium* spp. <sup>A</sup>Includes *Ilex anomala* and *Coprosma* spp. <sup>B</sup>Includes *Ilex anomala* and *Cheirodendron trigynum*. <sup>C</sup> $\alpha$  (thermal diffusivity) from thermocouple installed in tree fern used for CWD (fallen dead stems larger than 5 cm diameter) at both sites. <sup>D</sup> $\alpha$  for Nahuku used for *M. polymorpha* trees at ‘Ōla‘a.

Table 4.1. Summary of reported values of stand fresh biomass ( $B_F$ ), canopy height ( $Ht_{CANOPY}$ ), eddy covariance observation height ( $Ht_{OBS}$ ), heat storage terms, and energy closure improvements after inclusion of all heat storage terms.

Vegetation	$B_F$ ( $kg\ m^{-2}$ )	$Ht_{CANOPY}$ (m)	$Ht_{OBS}$ (m)	hourly max / min of mean diurnal cycle ( $W\ m^{-2}$ )						$\Omega$ / offset ( $W\ m^{-2}$ ) / $r^2$	
				$Q_B$	$Q_H$	$Q_{LE}$	$Q_S$	$Q_P$	$Q_{SUM}$	$R_{NET} - G$	$R_{NET} - G - Q_{SUM}$
<sup>A</sup> crop - maize	0 - 9	3	8	22	–	–	42	30	80 <sup>K</sup>	0.84 / 24 / 0.81	0.94 / 24 / 0.86
<sup>A</sup> crop - soybean	0 - 3.5	0.9	8	7	–	–	17	12	40 <sup>K</sup>	0.90 / 12 / 0.77	0.97 / 12 / 0.81
<sup>B</sup> deciduous broadleaf	39	27	46	18	35 / -9	4 / -4	35 / -9 <sup>J</sup>	–	69 / -30 <sup>L</sup>	–	0.72 / 0.96 / 0.92
<sup>C</sup> temperate eucalyptus	66 - 73	40	71.5	61 / -44	47 / -66	27 / -29	48 / -54 <sup>J</sup>	<3	51 / -55 <sup>K</sup>	0.90 / 0 / 0.88 <sup>M</sup>	1.01 / 0 / 0.87 <sup>M</sup>
<sup>D</sup> mid latitude grassland	1.7	0.1	3.5	–	–	–	–	–	–	0.90 / 0 / 0.95 <sup>M</sup>	0.96 / 0 / 0.97 <sup>M</sup>
<sup>E</sup> tropical forest	72.4	14 - 25	53.1	39 / -25	39 / -17	–	–	–	65 / -35 <sup>K</sup>	0.82 / 7.04 / 0.89	0.90 / -4 / 0.92
<sup>F</sup> Norway spruce - TH	39.9	30	42	14 / -10	15 / -11	4 / -6	1 / 0	8 / 0	33 / -21 <sup>K</sup>	0.75 / 21.8 / 0.92	0.81 / 18.6 / 0.92
<sup>F</sup> Norway spruce - RE	39.2	20 - 30	32	18 / -16	11 / -11	7 / -6	5 / -4	9 / 0	24 / 13 <sup>K</sup>	0.96 / 58.6 / 0.79	1.02 / 47.4 / 0.81
<sup>F</sup> Norway spruce - WS	39.2	20	30	9 / -5	7 / -7	3 / -3	3 / -2	9 / 0	20 / -7 <sup>K</sup>	0.67 / 16.0 / 0.92	0.70 / 14.9 / 0.92
<sup>F</sup> pine and spruce - NO	47.5	25	33	19 / -16	16 / -13	7 / -7	3 / -2	9 / 0	28 / -19 <sup>K</sup>	0.90 / 32.7 / 0.90	1.00 / 25.0 / 0.90
<sup>G</sup> pine and spruce - NO	43.4	28	35	22 / -20	15 / -14	5 / -8	15 / -4 <sup>J</sup>	–	40 / -35 <sup>L</sup>	0.857 / 9.9 / 0.92	0.975 / -2.3 / 0.95
<sup>H</sup> subalpine meadow	2.7 - 3.2	0.4	1.5	16 / -10	2 / -1	1 / -2	8 / -10	12 / -13	19 / -13 <sup>K</sup>	0.860 / 0 / 0.97 <sup>M</sup>	0.894 / 0 / 0.97 <sup>M</sup>
<sup>I</sup> tropical montane forest	69.8	17	25	27 / -18	8 / -6	7 / -4	–	–	38 / -26 <sup>L</sup>	0.767 / 0 / 0.93 <sup>M</sup>	0.805 / 0 / 0.93 <sup>M</sup>
<sup>I</sup> invaded tropical forest	75.9	12.5	18.3	48 / -29	8 / -4	7 / -3	–	–	56 / -33 <sup>L</sup>	0.918 / 0 / 0.94 <sup>M</sup>	0.997 / 0 / 0.94 <sup>M</sup>

<sup>A</sup> Meyers and Hollinger (2004), only daytime energy storage terms reported, therefore two hour maximum of mean diurnal cycle given; <sup>B</sup> Oliphant et al. (2004), dry biomass was given in the text, therefore fresh biomass was estimated by multiplying by 2. Mean diurnal cycle of storage terms is for April only; <sup>C</sup> Haverd et al. (2007), mean diurnal cycle of storage terms is only for day 73, 2005; <sup>D</sup> Jacobs et al. (2008); <sup>E</sup> Michiles and Gielow (2008), mean diurnal cycle of storage terms for the dry season only, heat flux plates were installed at 1 cm, hence  $Q_S$  was assumed to be small and therefore not measured; <sup>F</sup> Moderow et al. (2009), data from NO site from summer 2006; <sup>G</sup> Lindroth et al. (2010), data from same NO site from summer 1995; <sup>H</sup> Wang and Zhang (2011), <sup>I</sup> Nahuku and 'Ōla'a (this study). <sup>J</sup> includes G; <sup>K</sup>  $Q_{SUM}$  Does not include G; <sup>L</sup>  $Q_{SUM}$  includes G. <sup>M</sup> Y axis forced through zero.

A dash means that either the variable was not measured or not given. Some of the maximum and minimum hourly means of the diurnal cycle of storage terms were approximated from a figure in the relevant publication.

## FIGURES

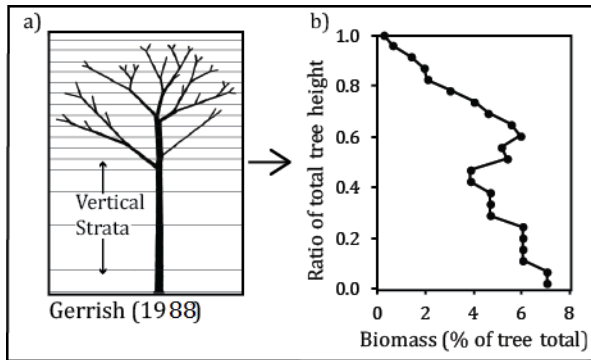


Figure 2.1. Stratified diagram of a mature *Metrosideros polymorpha* tree given by Gerrish (1988) (a), and the biomass height profile that was extrapolated from measurements of the stratified figure (b).

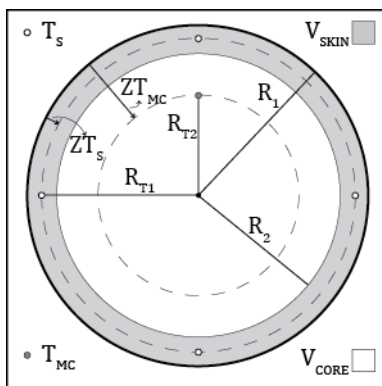


Figure 2.2. Cross-section of stem including variables used in radial separation of biomass.  $T_s$  ( $^{\circ}\text{C}$ ) are temperature measurements that are averaged to represent the annular portion of biomass ( $V_{SKIN}$ ,  $\text{cm}^3$ ),  $T_{MC}$  ( $^{\circ}\text{C}$ ) is the modeled stem core temperature that represents the volume of the interior of stems ( $V_{CORE}$ ,  $\text{cm}^3$ ),  $zT_s$  (1 cm in tree stems and 1.5 cm in *Cibotium* spp. stems) is the distance between the stem surface and the center of mass of  $V_{SKIN}$ ,  $zT_{MC}$  (cm) is the distance between the stem surface and the center of mass of  $V_{CORE}$ ,  $R_1$  (cm) is the radius of the stem,  $R_2$  (cm) is the radius of  $V_{CORE}$ ,  $R_{T1}$  (cm) is the distance between the center of the stem and the center of mass of  $V_{SKIN}$ , and  $R_{T2}$  (cm) is the distance between the center of the stem and the center of mass of  $V_{CORE}$ .

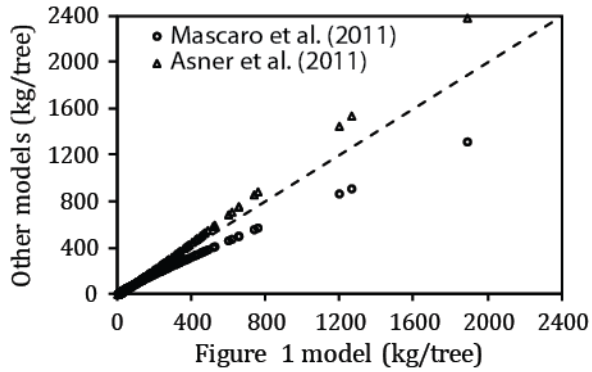


Figure 2.3. Bivariate association between biomass of surveyed trees predicted from the Figure 1 model with two published models of *Metrosideros* at Nahuku. The dashed line represents a 1:1 ratio between models.

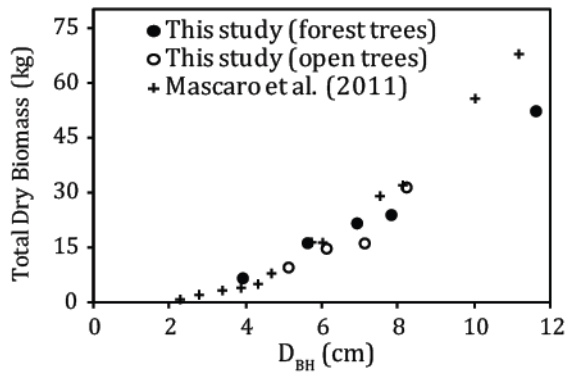


Figure 2.4. Dry biomass vs.  $D_{BH}$  (Diameter at 1.3 m) for all harvested *P. cattleianum* trees in this study ( $n=9$ ) and in Mascaro et al. (2011). Trees harvested under open canopy ( $n=4$ ) were not used in the allometric relationships described in Table 2.3.

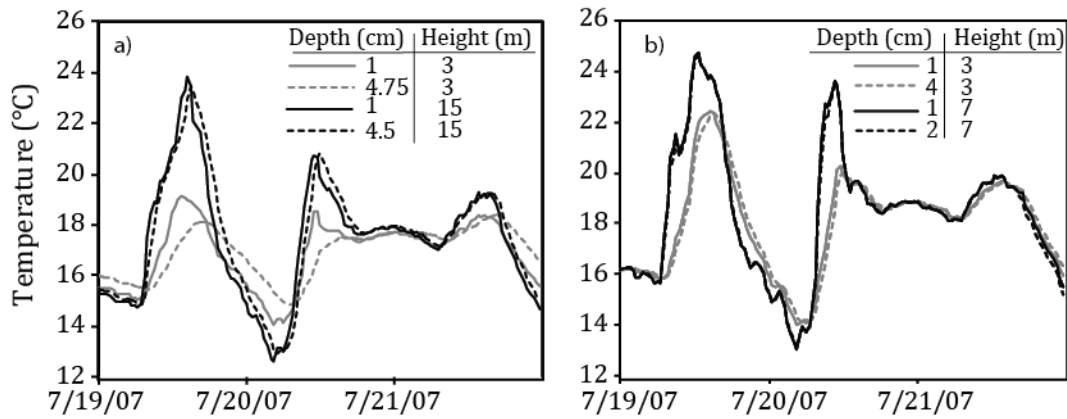


Figure 3.1. Three-day sample of stem temperature time series in a) *Metrosideros polymorpha* at Nahuku and b) *Psidium cattleianum* at 'Ōla'a. Mid-level tree stem temperature and *Cibotium* spp. stem temperature not shown. This period was chosen to exemplify large day-to-day variability.

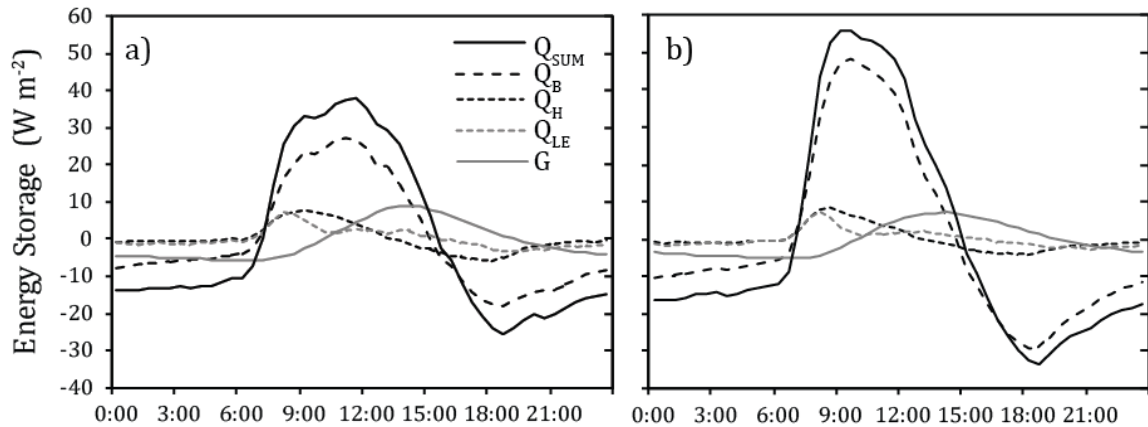


Figure 3.2. Mean diurnal cycle of heat storage in the biomass ( $Q_B$ ), sensible and latent energy storage in the air column below the eddy covariance sensors ( $Q_H$  and  $Q_{LE}$ , respectively), soil heat flux and energy storage in the top 8 cm of mineral soil ( $G$ ), and all heat storage terms combined ( $Q_{SUM}$ ) at Nahuku (a) and 'Ōla'a (b) averaged over the 34 months of analysis.

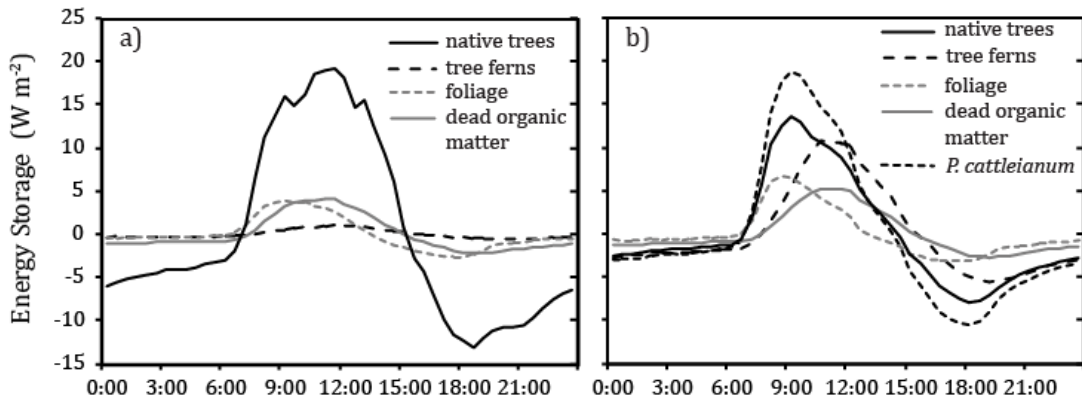


Figure 3.3. Mean diurnal cycles of heat storage in various biomass elements at Nahuku (a) and 'Ōla'a (b) averaged over the 34 months of analysis.

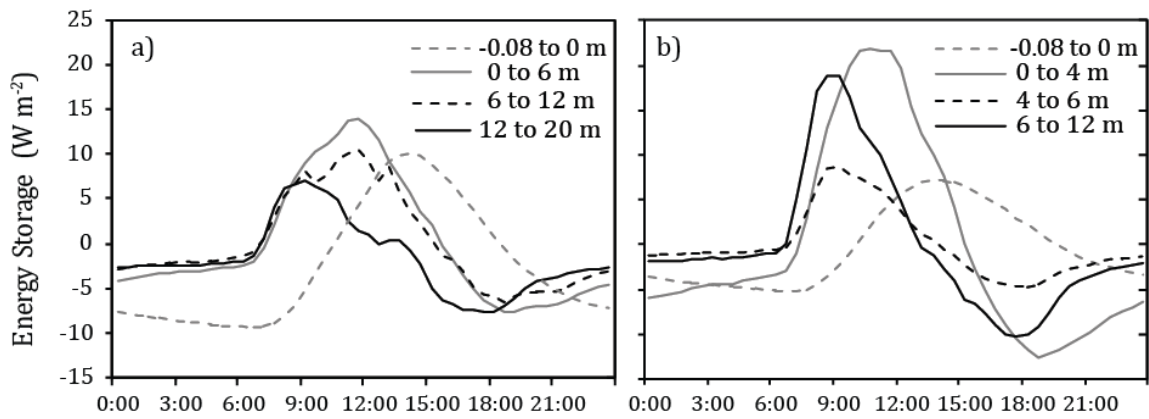


Figure 3.4. Mean diurnal cycles of the vertical distribution of heat storage in the biomass and the soil layer above the heat flux plates at Nahuku (a) and 'Ōla'a (b).

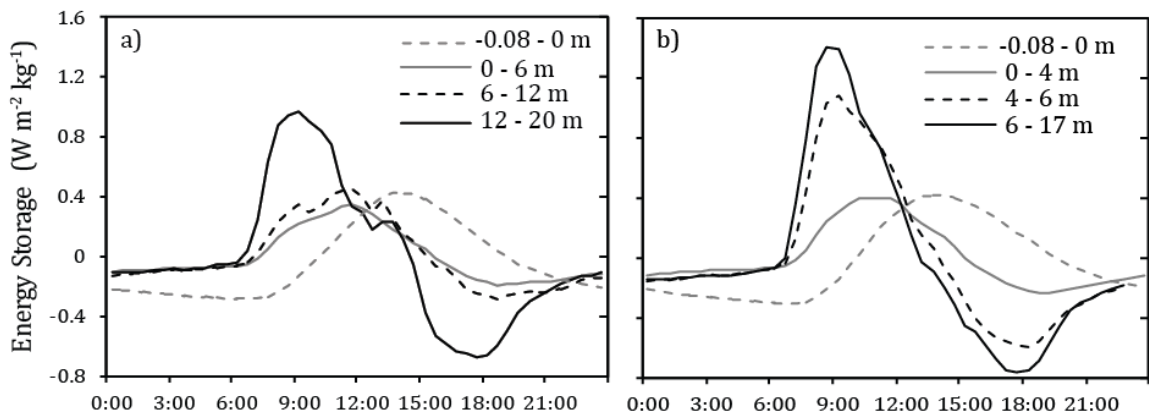


Figure 3.5. Mean diurnal cycle of mass specific heat storage at different levels in the canopy and the soil layer above the heat flux plates at Nahuku (a) and 'Ōla'a (b).

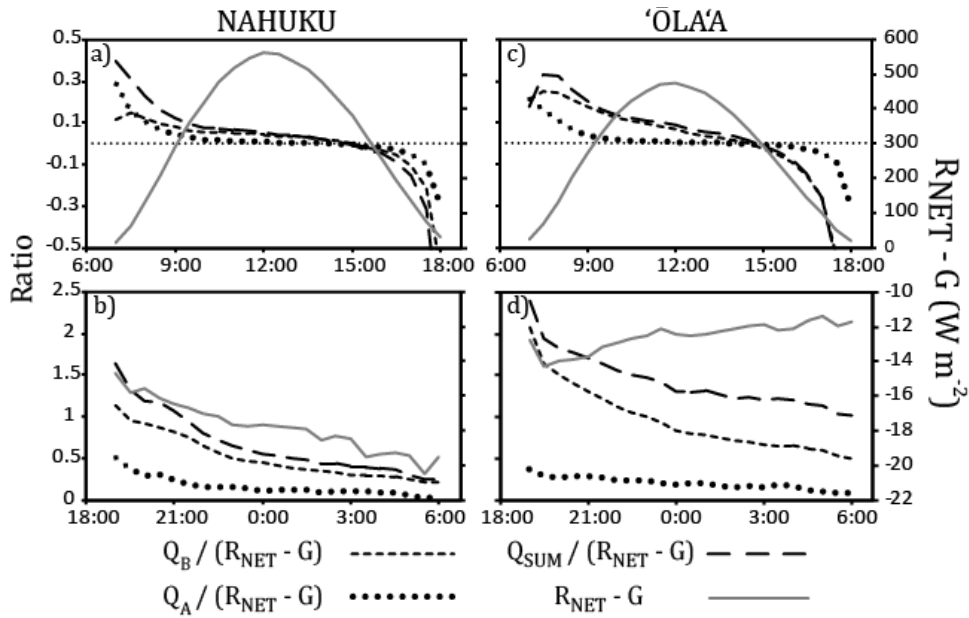


Figure 3.6. Mean diurnal cycles of the ratio's of the of heat storage in the biomass ( $Q_B$ ,  $W m^{-2}$ ), heat storage in the air layer below the eddy covariance sensors ( $Q_A$ ,  $W m^{-2}$ ), and all heat storage terms combined ( $Q_{SUM}$ ) to the mean diurnal cycle of net radiation minus soil heat flux ( $R_{NET} - G$ ,  $W m^{-2}$ ) at both sites for day (a, c) and night (b, d). For reference,  $R_{NET} - G$  is plotted on the right Y axis. Horizontal dotted line (a, c) represents a ratio of zero.

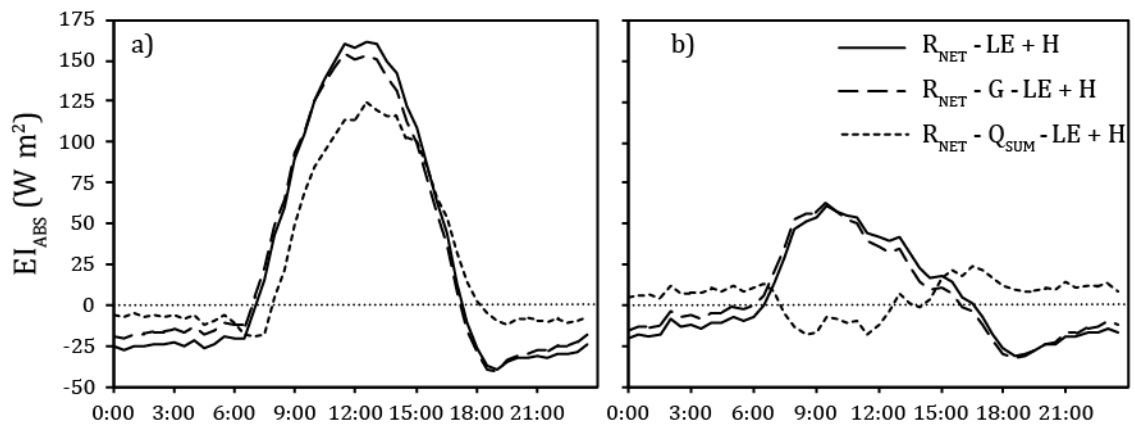


Figure 3.7. Mean diurnal cycles of absolute energy imbalance ( $EI_{ABS}$ ,  $W m^{-2}$ ) with and without heat storage terms at Nahuku (a) and 'Olā'a (b). Horizontal dotted lines represent a mean energy imbalance of zero  $W m^{-2}$ .

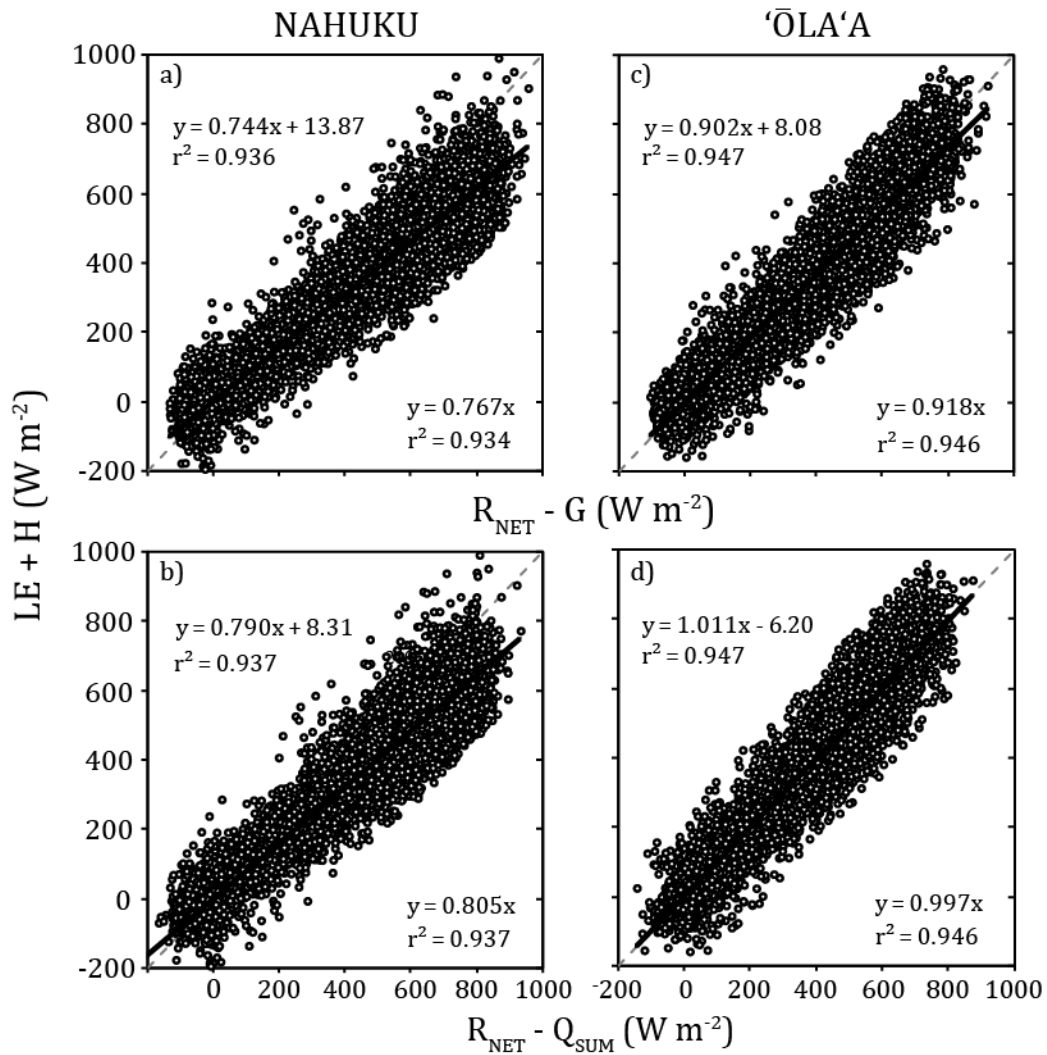


Figure 3.8. Scatterplots of the sum of turbulent flux vs. two versions of available energy, net radiation minus soil heat flux ( $R_{NET} - G$ ) and net radiation minus the sum of energy storage in the soil, biomass, and air ( $R_{NET} - Q_{SUM}$ ) at Nahuku and 'Ōla'a. Relative energy closure ( $\Omega$ ) is determined as the slopes of the best-fit lines shown. Regression equations on the bottom right of each figure are forced through the origin to express  $\Omega$  as one coefficient.

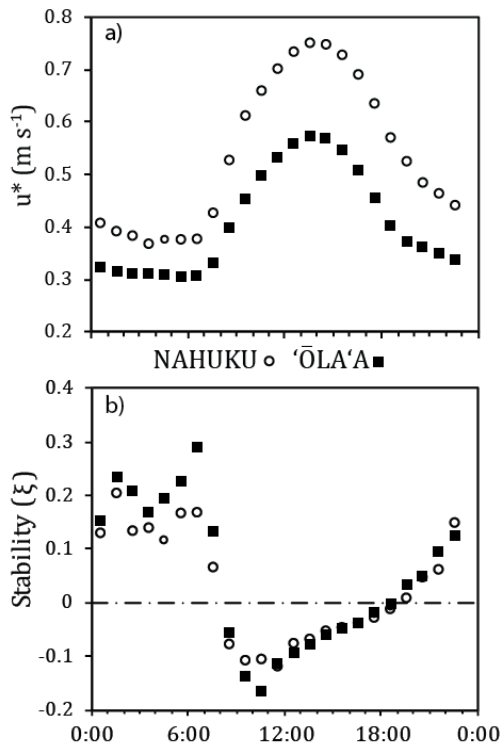


Figure 3.9. Mean diurnal cycles of friction velocity ( $u^*$ ) and stability ( $\xi$ ) at Nahuku and Ōla'a . The dashed line represents neutral stability.

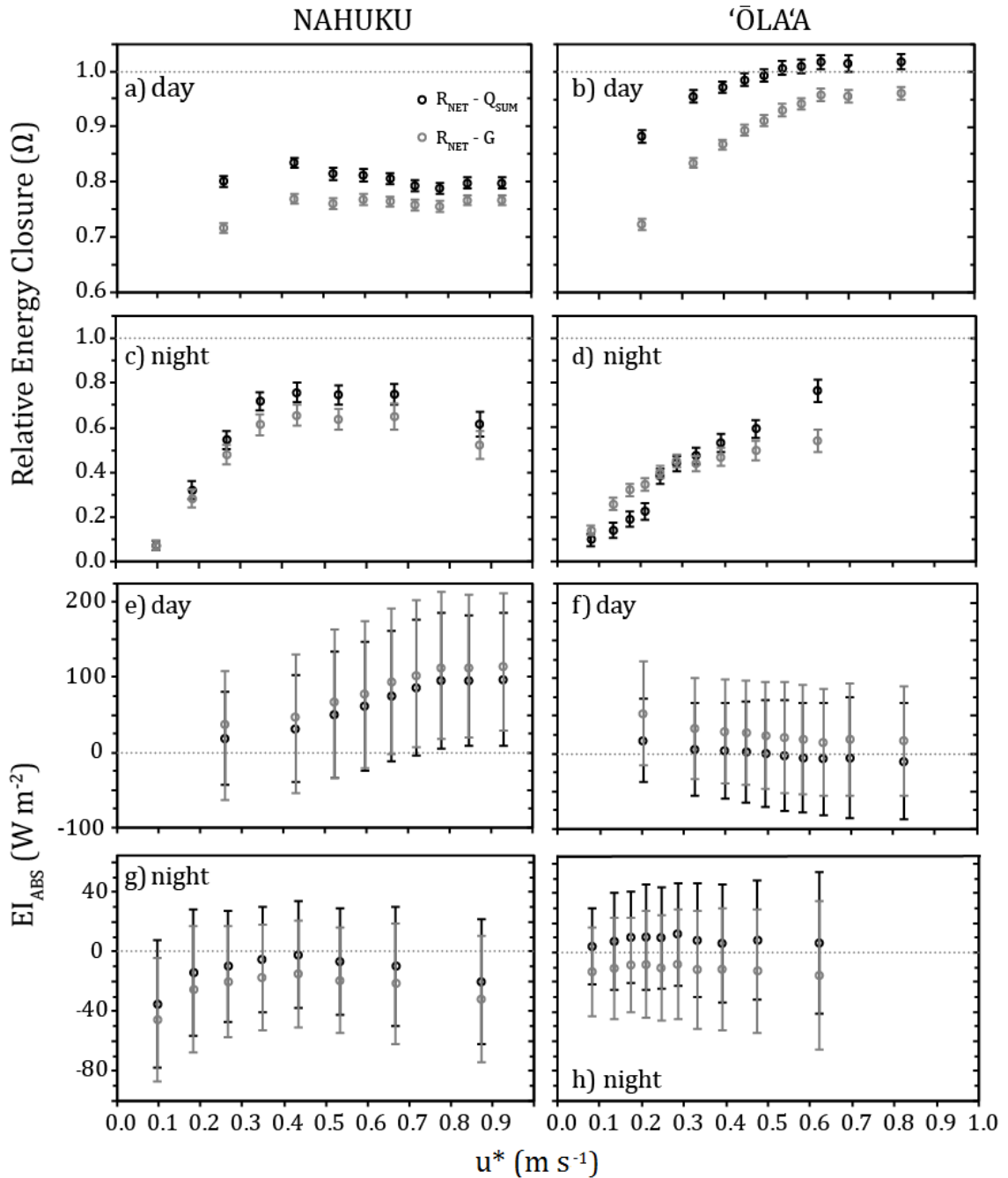


Figure 3.10.  $\Omega$  and  $EI_{ABS}$  as a function of  $u^*$  for Nahuku (a, c, e, and g) and 'Ōla'a (b, d, f, and h) for two cases: available energy is set to net radiation minus soil heat flux ( $R_{NET} - G$ ,  $W m^{-2}$ , gray circles) and available energy is set to net radiation minus the sum of energy storage in the soil, biomass, and air ( $R_{NET} - Q_{SUM}$ ,  $W m^{-2}$ , black circles). Data are plotted for even sized bins ( $n=500$  to  $1100$ ). Daytime and night-time data are shown separately. Error bars for a, b, c, and d represent  $\pm$  one standard error of the slope ( $S_B$ ), and for e, f, g, and h, error bars represent  $\pm$  one standard deviation. Horizontal dotted lines represent perfect energy closure.

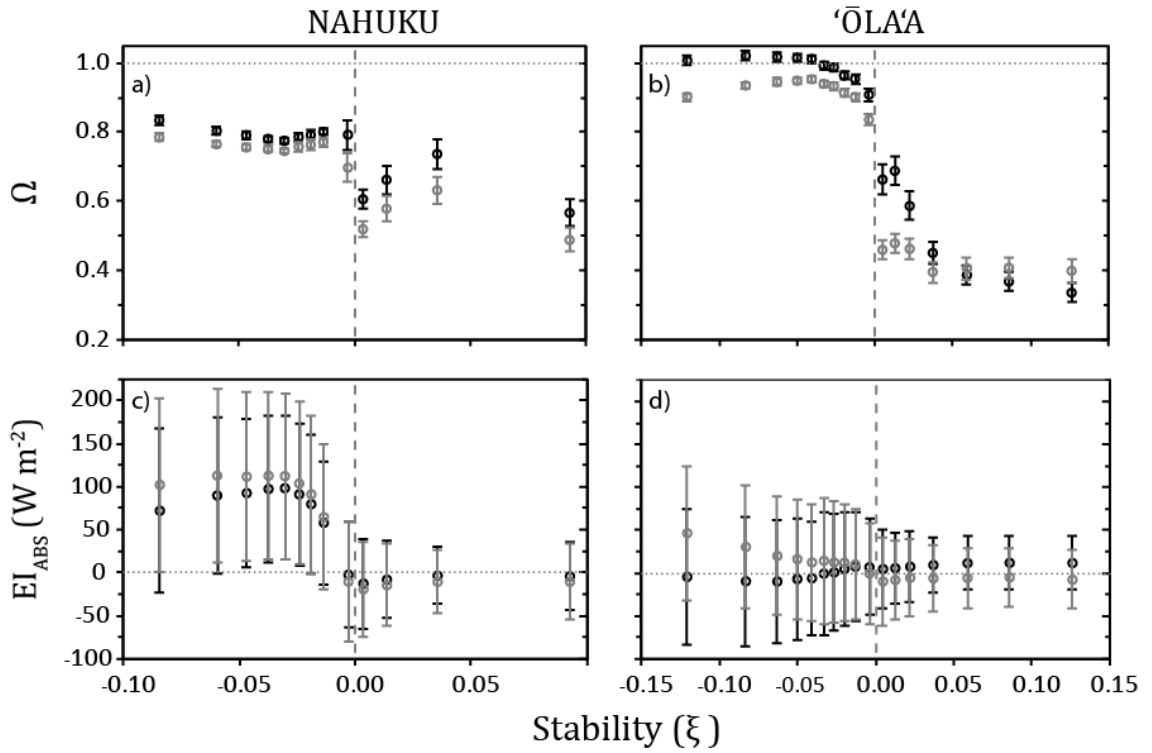


Figure 3.11. Relative energy closure ( $\Omega$ ) and the mean absolute energy imbalance ( $EI_{ABS}$ ) as a function of stability ( $\xi$ ) at Nahuku (a, c) and 'Ōla'a (b, d) for two cases: available energy is set to net radiation minus soil heat flux ( $R_{NET} - G$ ,  $W m^{-2}$ , gray circles) and available energy is set to net radiation minus the sum of energy storage in the soil, biomass, and air ( $R_{NET} - Q_{SUM}$ ,  $W m^{-2}$ , black circles) for even sized bins. Horizontal dotted lines represent perfect energy closure, and vertical dashed lines represent neutral atmospheric conditions. Error bars represent  $\pm$  one standard error of the slope ( $S_B$ ) for a and b, and  $\pm$  one standard deviation for c and d.

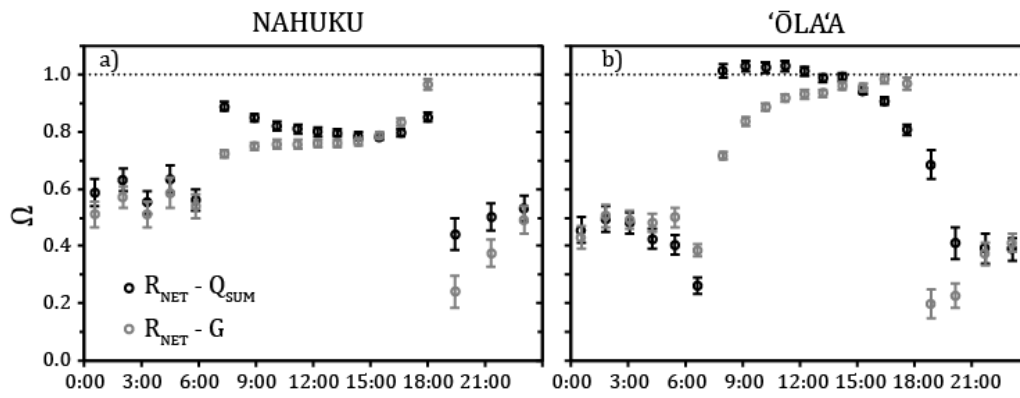


Figure 3.12. Relative energy closure ( $\Omega$ ) according to time of day for Nahuku (a) and Ōla'a (b) for two cases: 1) available energy is set to net radiation minus soil heat flux ( $R_{NET} - G$ ,  $W m^{-2}$ , gray circles), and available energy is set to net radiation minus the sum of energy storage in the soil, biomass, and air ( $R_{NET} - Q_{SUM}$ ,  $W m^{-2}$ , black circles) for even sized bins. Horizontal dotted lines represent perfect energy closure. Error bars represent the standard error of the slope ( $S_B$ ).